NAVAL POSTGRADUATE SCHOOL
MONTEREY, CALIFORNIA

THESIS

EFFECT OF FLUID MESH TRUNCATION ON THE RESPONSE OF A FLOATING SHOCK PLATFORM (FSP) SUBJECTED TO AN UNDERWATER EXPLOSION (UNDEX)

by

James R. Smith

September 1999

Thesis Advisor: Young S. Shin

Approved for public release; distribution is unlimited.

19991227 032

REPORT DOCUMENTATION PAGE		Form Approved OMB No. 0704-0188

Public reporting burden for this collection of information is estimated to average 1 hour per response, including the time for reviewing instruction, searching existing data sources, gathering and maintaining the data needed, and completing and reviewing the collection of information. Send comments regarding this burden estimate or any other aspect of this collection of information, including suggestions for reducing this burden, to Washington Headquarters Services, Directorate for Information Operations and Reports, 1215 Jefferson Davis Highway, Suite 1204, Arlington, VA 22202-4302, and to the Office of Management and Budget, Paperwork Reduction Project (0704-0188) Washington DC 20503.

1. AGENCY USE ONLY *(Leave blank)*	2. REPORT DATE September 1999.	3. REPORT TYPE AND DATES COVERED Master's Thesis	
4. TITLE AND SUBTITLE: EFFECT OF FLUID MESH TRUNCATION ON THE RESPONSE OF A FLOATING SHOCK PLATFORM (FSP) SUBJECTED TO AN UNDERWATER EXPLOSION (UNDEX)			**5. FUNDING NUMBERS**
6. AUTHOR(S) Smith, James R. LT/USN			
7. PERFORMING ORGANIZATION NAME(S) AND ADDRESS(ES) Naval Postgraduate School Monterey CA 93943-5000			**8. PERFORMING ORGANIZATION REPORT NUMBER**
9. SPONSORING/MONITORING AGENCY NAME(S) AND ADDRESS(ES)			**10. SPONSORING/MONITORING AGENCY REPORT NUMBER**

11. SUPPLEMENTARY NOTES
The views expressed here are those of the authors and do not reflect the official policy or position of the Department of Defense or the U.S. Government.

12a. DISTRIBUTION/AVAILABILITY STATEMENT Approved for public release; distribution is unlimited.	12b. DISTRIBUTION CODE

13. ABSTRACT *(maximum 200 words)*

Shock trials are required for the lead ship of each new construction shock hardened ship class. The Navy's Floating Shock Platform (FSP) is used in the acceptance of mission-essential items for installation aboard shock hardened ships if the size and weight of the item permits such testing. Live fire shock trials and underwater explosion testing are both complex and expensive. Finite element modeling and simulation provides a viable, cost effective alternative to these tests. This thesis investigates the effects of reducing the amount of fluid mesh required to accurately capture the structural response of a finite element model of the FSP subjected to an underwater explosion. This same approach can be applied to a finite element model of each shock hardened ship class. With reliable results, computer simulation of ship shock trials and underwater explosion testing could become a dependable, cost effective, and time efficient manner for validating surface ship shock hardening requirements.

14. SUBJECT TERMS Underwater Explosion, Floating Shock Platform		15. NUMBER OF PAGES 86
		16. PRICE CODE

17. SECURITY CLASSIFICATION OF REPORT Unclassified	18. SECURITY CLASSIFICATION OF THIS PAGE Unclassified	19. SECURITY CLASSIFICATION OF ABSTRACT Unclassified	20. LIMITATION OF ABSTRACT UL

NSN 7540-01-280-5500

Standard Form 298 (Rev. 2-89)
Prescribed by ANSI Std. 239-18 298-102

EFFECT OF FLUID MESH TRUNCATION ON THE REPONSE OF A FLOATING SHOCK PLATFORM (FSP) SUBJECTED TO AN UNDERWATER EXPLOSION (UNDEX)

James R. Smith
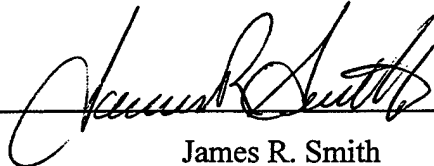Lieutenant, United States Navy
B.A., University of Washington, 1991

Submitted in partial fulfillment of the
Requirements for the degree of

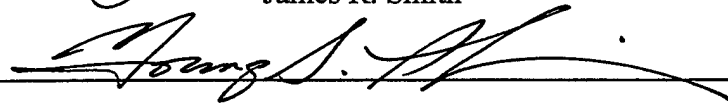## MASTER OF SCIENCE IN MECHANICAL ENGINEERING

from the

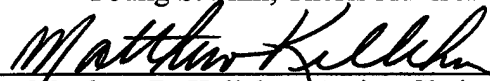## NAVAL POSTGRADUATE SCHOOL
September 1999

Author: _____
James R. Smith

Approved by: _____
Young S. Shin, Thesis Advisor

_____
Matthew D. Kelleher, Acting Chairman
Department of Mechanical Engineering

ABSTRACT

Shock trials are required for the lead ship of each new construction shock hardened ship class. The Navy's Floating Shock Platform (FSP) is used in the acceptance of mission-essential items for installation aboard shock hardened ships if the size and weight of the item permits such testing. Live fire shock trials and underwater explosion testing are both complex and expensive. Finite element modeling and simulation provides a viable, cost effective alternative to these tests. This thesis investigates the effects of reducing the amount of fluid mesh required to accurately capture the structural response of a finite element model of the FSP subjected to an underwater explosion. This same approach can be applied to a finite element model of each shock hardened ship class. With reliable results, computer simulation of ship shock trials and underwater explosion testing could become a dependable, cost effective, and time efficient manner for validating surface ship shock hardening requirements.

TABLE OF CONTENTS

LIST OF FIGURES

x

ACKNOWLEDGEMENTS

I. INTRODUCTION

A. BACKGROUND

Since September 1992, the Department of the Navy's strategic planning document [Ref. 1] has officially required U.S. forces to be ready to operate in "littoral" or shallow water environments instead of the open-ocean climates it had based it's warfighting strategies on previously. This change in policy significantly increased the potential for relatively inexpensive weapons, such as underwater mines, to be purchased and layed in the "littoral" environments U.S. Navy warships now routinely patrol. The underwater explosion from one of these weapons can produce shock waves or pressure pulses that, when applied to the large area of the ship's hull, can have a serious negative effect on the ship's structure and equipment, as well as causing serious personnel casualties. However, this is not a new concern. As a defensive measure, the U.S. Navy, since the Second World War, has been developing guidelines and specifications for the shock testing and hardening of shipboard equipment and systems. NAVSEA 0908-LP-000-3010A [Ref. 2] and MIL-S-901D [Ref. 3] are examples of this guidance. The shock resistance validation is then conducted through shock trials as required in OPNAVINST 9072.2 [Ref. 4]. At this time, shock trials are the only means of testing a ship and it's mission-critical systems under combat-like conditions short of an actual conflict. These trials are required for the lead ship of each new construction shock hardened ship class. These requirements have since proved their worth, when in 1991 during Operation Desert Storm, the USS Princeton (CG-59) struck a floating mine near the bow causing severe hull girder damage near the stern of the ship and only minor personnel casualties. There may have been massive loss of life as well as the complete loss of the ship had it not been for the heroic damage control efforts, as well as the "shock hardening" design requirements mandated by the Department of the Navy.

Unfortunately, conducting ship shock trials can be time consuming and expensive. Initial planning stages for the shock trial of the USS John Paul Jones (DDG 53) began four years prior to the actual test date while the ship was still undergoing construction at Bath Iron Works, Maine. The entire endeavor involved over 50 government agencies.

1

Originally scheduled for February 1994, the shock trial was delayed 3 months due to a lawsuit filed against the Navy by environmentalist groups concerned over the well being of sea life in the testing area. When testing occurred in June 1994, only two of the four required tests could be carried out because of inclement weather. The remaining two shock tests could not be performed. Further modifications to the ship's schedule to accommodate the two tests were not feasible since the three-month delay had already affected the ship's post trial delivery date and deployment preparations [Ref. 5].

With the advent and ongoing advances in computer technology, finite element modeling and simulation has become a viable, less costly alternative to live fire testing. Finite element modeling using codes such as True*Grid*® [Ref. 6] and MSC/PATRAN [Ref. 7] have enabled the generation of detailed finite element models in a timely manner. To analyze finite element models, highly detailed model meshes are required to provide the most reliable results. An important aspect of this model detail is the inclusion of the surrounding fluid in order to accurately capture the response of the ship caused by the impact of the shock wave. The fluid mesh must be constructed to mate exactly with the finite element mesh of the structure and must be of sufficient size to capture the bulk cavitation zone. However, depending on the size of the charge producing the underwater explosion event, as well the depth of the charge, this bulk cavitation zone can become quite large. The larger the cavitation zone, the greater the number of finite elements required to accurately model the fluid. Subsequently, greater computational memory and time are required to perform the structural analysis.

B.   SCOPE OF RESEARCH

This paper investigates the effects of reducing the fluid mesh size on the accuracy of the structural response of a finite element model subjected to an underwater explosion. The model to be considered in this study is of the Navy's Floating Shock Platform (FSP). The FSP is used in the acceptance of mission-essential items for installation aboard shock hardened ships if the size and weight of the item permits such testing [Ref. 4]. Analysis of the model response is conducted using the LS-DYNA/USA (Underwater Shock

2

Analysis) coupled computer code [Ref.'s 13 and 14]. The purpose of this thesis is to compare the responses of truncated or reduced fluid mesh size models to that of a full size model, which is comprised of fluid volume elements within the bulk cavitation zone, as well as elements outside of the cavitation zone, closer to the location of the explosive charge. With reliable results, computer simulation of ship shock trials could become a dependable, cost effective, and time efficient manner for validating surface ship shock hardening requirements.

THIS PAGE INTENTIONALLY LEFT BLANK

II. UNDERWATER EXPLOSIONS

A.   UNDERWATER SHOCK PHENOMENA

An underwater explosion occurs in a complex sequence of events. When a high explosive, such as TNT or HBX-1 is detonated, the original solid material of the explosive is converted into a very high temperature and pressure gas within nanoseconds (on the order of 3000°C and 50000 atm.) [Ref. 8]. The pressure wave that is formed originates in one section of the explosive and propagates throughout the remainder of the explosive. As this pressure wave propagates, it initiates the chemical reaction that creates more pressure waves. The pressure wave velocity steadily increases within the solid explosive until it exceeds the speed of sound in the explosive, creating a shock wave. The shock wave propagates through the solid at a constant speed and then, with the high temperature and pressure behind the shock front, into the surrounding medium [Ref. 9].

The high-pressure gas that results from the explosion rapidly expands outward in a radial manner, Fig. 1, and imparts an outward velocity on the surrounding water as
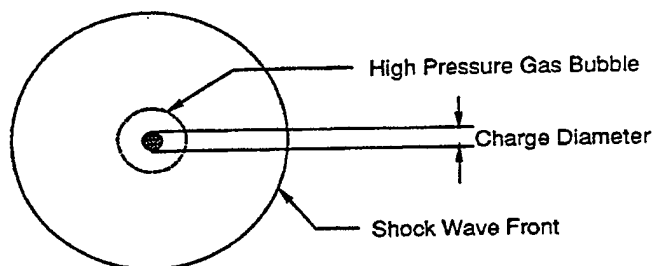
Figure 1. Gas Bubble and Shock Wave from an Underwater Explosion

well. Initially, the pressure is much greater than the atmospheric and hydrostatic pressure that opposes it and is therefore compressive in nature. At detonation, the pressure rise produces a steep fronted discontinuous wave, which decays exponentially with time as shown in Fig. 2. Duration of the pressure disturbance lasts only a few milliseconds. The

5

shock wave is assumed to propagate at several times that of the speed of sound in water, approximately 5,000 ft/sec, near the charge, which then falls rapidly to acoustic velocity as it travels outward in the water.
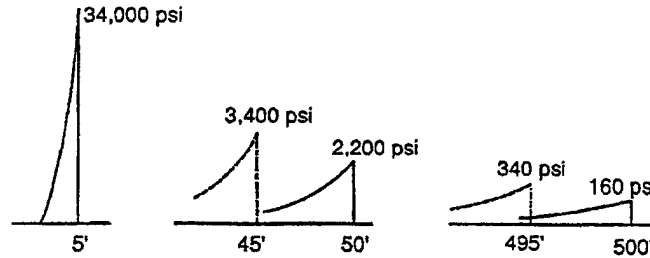
Figure 2. Shock Wave Profiles From a 300 lb. TNT Charge [Ref. 8]

Additionally, the pressure profile of the shock wave is proportional to the inverse of the distance from the charge, 1/d, and the wave profile gradually broadens as it spreads out [Ref. 8]. Empirical equations have been determined to define the profile of the shock wave. These relations enable calculation of the pressure profile of the shock wave (P(t)), the maximum pressure of the wave (P_{max}), the shock wave decay constant (θ), the bubble period (T), and the maximum bubble radius (A_{max}).

$$P(t) = P_{max} e^{-\frac{t-t_1}{\theta}} \quad \text{(psi)} \tag{2.1}$$

$$P_{max} = K_1 \left(\frac{W^{\frac{1}{3}}}{R} \right)^{A_1} \quad \text{(psi)} \tag{2.2}$$

$$\theta = K_2 W^{\frac{1}{3}} \left(\frac{W^{\frac{1}{3}}}{R} \right)^{A_2} \quad \text{(msec)} \tag{2.3}$$

$$T = K_5 \frac{W^{\frac{1}{3}}}{(D+33)^{\frac{5}{6}}} \quad \text{(sec)} \tag{2.4}$$

6

$$A_{max} = K_6 \frac{W^{\frac{1}{3}}}{(D+33)^{\frac{1}{3}}} \quad \text{(ft)} \quad\quad\quad (2.5)$$

Other variables in the equations are:

W = Charge weight (lbf)

R = Standoff distance (ft)

D = Charge depth (ft)

t_1 = arrival time of shock wave (msec)

t = time of interest (msec)

$K_1, K_2, K_5, K_6, A_1, A_2$ = Shock wave parameters

Through calculation, it can be determined that P_{max} decreases by approximately one-third after one decay constant.

Subsequent pressure waves or bubble pulses are generated by the oscillation of the gas bubble created by the underwater explosion. The peak pressure of the first bubble pulse is approximately 10-20% of the shock wave, but is of greater duration making the area under both pressure curves similar [Ref. 9]. The bubble expands until dynamic equilibrium is reached . The bubble then contracts until dynamic equilibrium is again reached, followed by another expansion. This oscillation sequence continues until the energy of the reaction is dissipated or the bubble reaches the free surface or impacts the target.

Depending on the charge location relative to the surface and the bottom, other effects are characteristic of an underwater shock. Bottom reflection is the bouncing of the shock wave off of the bottom of the body of water; a compressive wave. Refraction causes the shock wave to travel through the bottom of the body of water before emerging again; also a compressive wave. In reasonably deep water, these two effects are not usually an issue for surface vessels.

Free surface reflection is a very important effect, however. This reflected wave is tensile in nature, as opposed to the other compressive wave effects, and is produced from the rarefaction of the shock wave from the free surface. This rarefaction wave contributes to the creation of bulk cavitation.

B.   FLUID-STRUCTURE INTERACTION

When an object such as a ship or submarine is in the vicinity of an underwater explosion, the shock pressure pulses produced by the explosion impinge upon the surface of the structure. A fluid-structure interaction takes place as the pressure pulse acts upon the flexible surface of the structure. This dynamic response of the a linear elastic structure in the fluid can be expressed by:

$$[M_s]\{\ddot{x}\} + [C_s]\{\dot{x}\} + [K_s]\{x\} = \{f\} \tag{2.6}$$

where $[M_s]$ is the mass matrix, $[C_s]$ is the dampening matrix, $[K_s]$ is the stiffness matrix, $\{\ddot{x}\}$ is the acceleration vector, $\{\dot{x}\}$ is the velocity vector, and $\{x\}$ is the displacement vector of the structure and $\{f\}$ is the external force vector. In the case of a submerged structure excited by an acoustic wave, $\{f\}$ is given by:

$$\{f\} = -[G][A_f](\{p_I\} + \{p_S\}) + \{f_D\} \tag{2.7}$$

where $[G]$ is the transformation matrix that relates the surface nodal forces of the fluid and structure, $[A_f]$ is the diagonal area matrix associated with the fluid elements, $\{p_I\}$=incident wave nodal pressure vector, and $\{p_S\}$=scattered wave nodal pressure vector [Ref. 11].

The Doubly Asymptotic Approximation (DAA) method was developed in 1971 [Ref. 10], which described a matrix of differential equations in time for the approximation of acoustic fluid-structure interaction. This approximation was so named because it is accurate at both low and high frequencies and at early and late times. The DAA represents the surrounding fluid of the structure through the interaction of state variables pertaining only to the structure's wet surface. The fluid equation of the DAA is

8

$$[M_f]\{\dot{p}_S\} + \rho c[A_f]\{p_S\} = \rho c[M_f]\{\ddot{u}_S\} \qquad (2.8)$$

where $[M_f]$ is the symmetric fluid mass matrix for the wet-surface fluid mesh, $\{p_S\}$ and $\{\dot{p}_S\}$ are the nodal pressure vector and its first time derivative of the scattered wave, c is the acoustic velocity of water, $[A_f]$ is the diagonal area matrix associated with the fluid elements, and $\{\ddot{u}_S\}$ is the scattered wave velocity vector. An object in the fluid will have a structural response defined as follows in Eq. (2.9),

$$[M_s]\{\ddot{x}\} + [C_s]\{\dot{x}\} + [K_s]\{x\} = \{f\} \qquad (2.9)$$

where $[M_s]$ is the mass matrix, $[C_s]$ is the dampening matrix, $[K_s]$ is the stiffness matrix, $\{\ddot{x}\}$ is the acceleration vector, $\{\dot{x}\}$ is the velocity vector, and $\{x\}$ is the displacement vector of the structure and $\{f\}$ is the external force vector.

The kinematic compatibility relation can then be applied to relate $\{u_S)$ to the structural response,

$$[G]^T\{\dot{x}\} = \{u_I\} + \{u_S\} \qquad (2.10)$$

The "T" superscript indicates the transpose of the matrix. This equation is an expression of the constraint that the normal fluid particle velocity must match the normal structural velocity on the structure wetted surface.

Substituting Equation (2.7) into (2.6) and Equation (2.10) can be substituted into (2.8) resulting in Equations (2.11) and (2.12),

$$[M_s]\{\ddot{x}\} + [C_s]\{\dot{x}\} + [K_s]\{x\} = -[G][A_f](\{p_I\} + \{p_S\}) \qquad (2.11)$$

and

$$[M_f]\{\dot{p}_S\} + \rho c[A_f]\{p_S\} = \rho c[M_f]([G]^T\{\ddot{x}\} - \{\dot{u}_I\}) \qquad (2.12)$$

The Underwater Shock Analysis (USA) code solves Eqs. (2.11) and (2.12) simultaneously by using a staggered solution procedure that is unconditionally stable with respect to the time step used [Ref. 11]. Once this system of equations is solved, desired response results such as displacement, velocity, and acceleration can be studied.

9

C.   CAVITATION

Two types of cavitation can occur during an UNDEX event. "Local cavitation" occurs at the fluid-structure interface and "bulk cavitation" occurs near the free surface and can cover a relatively large area. A discussion of both forms of cavitation follow below.

1.   Local Cavitation

Taylor flat plate theory, the simplest case of fluid-structure interaction is used to illustrate how local cavitation occurs. In this case, an infinite, air-backed plate is acted upon by an incident plane shock wave as shown below in Fig. 3.
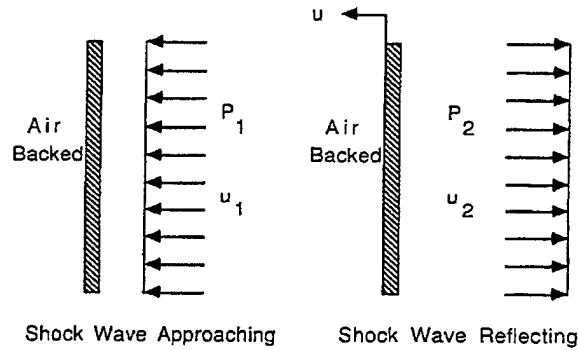
Figure 3. Taylor Plate Subjected to a Plane Wave [Ref. 9]

Once the shock wave strikes the plate, a reflected shock wave leaves the plate. According to Newton's second law of motion as shown in Eq. (2.13),

$$m\frac{du}{dt} = P_1 + P_2 \qquad (2.13)$$

where m is the mass of the plate per unit area, u is the velocity of the plate after being subjected to the shock wave, $P_1(t)$ is the incident wave pressure and $P_2(t)$ is the reflected, or scattered, wave pressure. Define the fluid particle velocities behind the incident and reflected shock waves as $u_1(t)$ and $u_2(t)$. The velocity of the plate is then defined by Eq. (2.14),

$$u(t) = u_1(t) - u_2(t) \tag{2.14}$$

For the one dimensional plane wave, the wave equation is $P = \rho Cu$. It follows that the incident and reflected shock wave pressures, Eqs. (2.15) and (2.16), are

$$P_1 = \rho Cu_1 \tag{2.15}$$

$$P_2 = \rho Cu_2 \tag{2.16}$$

where ρ is the fluid density and C is the acoustic velocity in water. Substituting the above pressure Eqs (2.15) and (2.16) into the velocity Eq. (2.14) results in the incident shock pressure being defined as Eq. (2.17)

$$P_1(t) = P_{max} e^{-\frac{t}{\theta}} \tag{2.17}$$

Solving for the reflected shock pressure yields Eq. (2.18),

$$P_2(t) = P_1 - \rho Cu = P_{max} e^{-\frac{t}{\theta}} - \rho Cu \tag{2.18}$$

where t is the time after the shock wave arrives at the target. Now the equation of motion, Eq. (2.13) can be rewritten as Eq. (2.19),

$$m\left(\frac{du}{dt}\right) + \rho Cu = 2P_{max} e^{-\frac{t}{\theta}} \tag{2.19}$$

which is a first order, linear differential equation. The solution, u(t), of the differential equation is expressed in Eq. (2.20) as

$$u = \frac{2P_{max}\theta}{m(1-\beta)} [e^{-\frac{\beta t}{\theta}} - e^{-\frac{t}{\theta}}] \tag{2.20}$$

with $\beta = \rho C\theta/m$ and $t>0$. The total pressure that impinges on the plate is defined as Eq. (2.21),

$$P_1 + P_2 = P_{max} [\frac{2}{1-\beta} e^{-\frac{t}{\theta}} - \frac{2\beta}{1-\beta} e^{-\frac{\beta t}{\theta}}] \tag{2.21}$$

11

As the value of β becomes larger, as in the case of a lightweight plate, the total pressure will become negative at a very early time. However, since water cannot support tension, negative pressure cannot exist. Therefore, as the water pressure reduces to vapor pressure at the surface of the plate, cavitation occurs. At this point, the pressure in front of the plate has been cut off and the plate has reached its maximum velocity [Ref. 9].

A ship's hull can be easily generalized as a Taylor flat plate. Local cavitation is likely to occur along the hull where the pressure pulse from the UNDEX impinges with sufficient force and the hull plating β value is large enough to make the net pressure negative.

2. Bulk Cavitation

The incident shock wave is compressive in nature. A rarefaction wave, which is tensile in nature, is created when the shock wave is reflected from the free surface. Since water cannot sustain a significant amount of tension, cavitation will occur when the pressure drops to zero or below. Upon cavitation, the water pressure rises to the vapor pressure of water, approximately 0.3 psi. This cavitated region created by the rarefaction wave is known as the bulk cavitation zone. It consists of an upper and lower boundary and its extent is dependent on the charge size, type, and depth [Ref.'s 18 - 20].

Figure 4 shows a typical bulk cavitation zone. The cavitation zone is symmetric about the y-axis in the figure; typically only one-half is shown due to the symmetry. The water particles behind the shock wave front at the time of cavitation have velocities depending on their location relative to the charge and the free surface. Water particles near the free surface, for example, will have a primarily vertical velocity at cavitation. As the reflected wave passes, the particles will be acted upon by gravity and atmospheric pressure.

The upper cavitation boundary is the set of points where the rarefaction wave passes and reduces the absolute pressure to zero or a negative value. The region will remain cavitated as long as the pressure remains below the vapor pressure. The total or absolute pressure, which determines the upper boundary, is a combination of atmospheric

pressure, hydrostatic pressure, incident shock wave pressure, and rarefaction wave pressure.
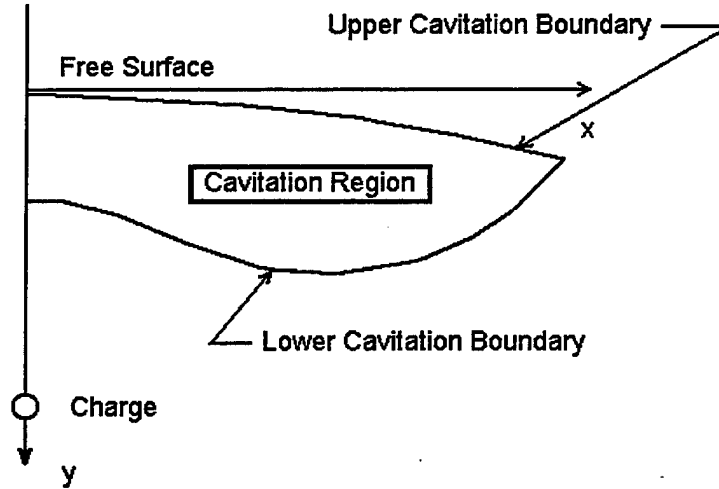
Figure 4. Bulk Cavitation Zone [Ref. 9]

The lower cavitation boundary is determined by equating the decay rate of the breaking pressure to the decay rate of the total absolute pressure. The breaking pressure is the rarefaction wave pressure that reduces a particular location of a fluid to the point of cavitation pressure, or zero psi.

The upper and lower cavitation boundaries can be calculated from Equations (2.22) and (2.23), respectively [Ref. 19]. Any point which satisfies F(x,y) and G(x,y) = 0 determines the bulk cavitation boundary.

$$F(x,y) = K_1 \left(\frac{W^{\frac{1}{3}}}{r_1} \right)^{A_1} e^{-\frac{(r_2 - r_1)}{\theta}} + P_A + \gamma y - K_1 \left(\frac{W^{\frac{1}{3}}}{r_2} \right)^{A_1} \tag{2.22}$$

$$G(x,y) = -\frac{P_i}{C\theta} \left\{ 1 + \left[\frac{r_2 - 2D\left(\frac{D+y}{r_2} \right)}{r_1} \right] \left[\frac{A_2 r_2}{r_1} - A_2 - 1 \right] \right\} - \tag{2.23}$$

$$\frac{A_1 P_i}{r_1^2} \left[r_2 - 2D\left(\frac{D+y}{r_2} \right) \right] + \gamma \left(\frac{D+y}{r_2} \right) + \frac{A_1}{r_2} (P_i + P_a + \gamma y) \qquad -$$

13

The variables in Equations (2.22) and (2.23) are:

x, y = horizontal range and vertical depth of the point

r_1 = standoff distance from the charge to the point

r_2 = standoff distance from the image charge to the point

C = acoustic velocity in the water

D = charge depth

θ = decay constant

γ = weight density of water

P_A = atmospheric pressure

W = charge weight

P_i = P(t), Equation (2.1)

θ = Equation (2.3)

K_1, A_1 = shock wave parameters

Figure 5 shows the charge geometry for the above two equations.
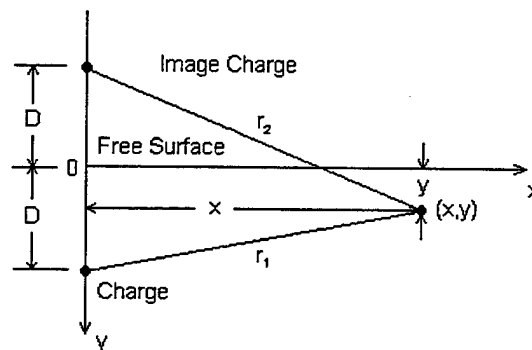
Figure 5. Charge Geometry for Bulk Cavitation Equations [Ref. 9]

Appendix A provides a MATLAB m-file [Ref. 12] that calculates and plots the bulk cavitation zone for a user supplied charge weight (of HBX-1) and depth by solving

14

Equations (2.22) and (2.23). Figure 6 provides an example of cavitation curves generated using the program for two different charge weights at three different depths.
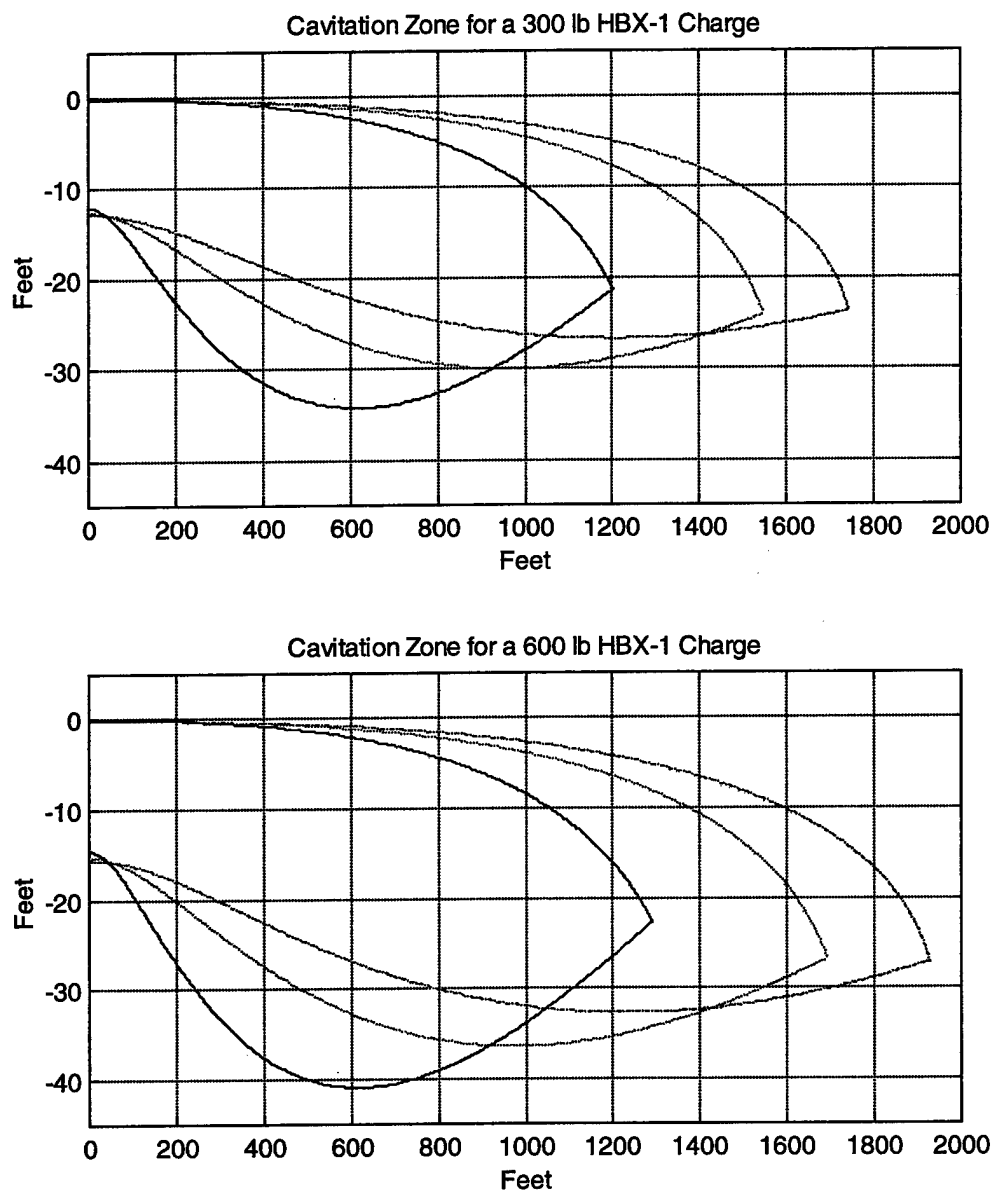
Figure 6. Bulk Cavitation Zones for HBX-1 Charges at the Following Depths:
— 100 ft, -- 200 ft, -. 300 ft

THIS PAGE INTENTIONALLY LEFT BLANK

III. MODELING

Modeling and testing involves model construction and pre-processing, analysis and solution, and post-processing programs. A flow chart of the model building and testing procedure is shown below in Figure 7.
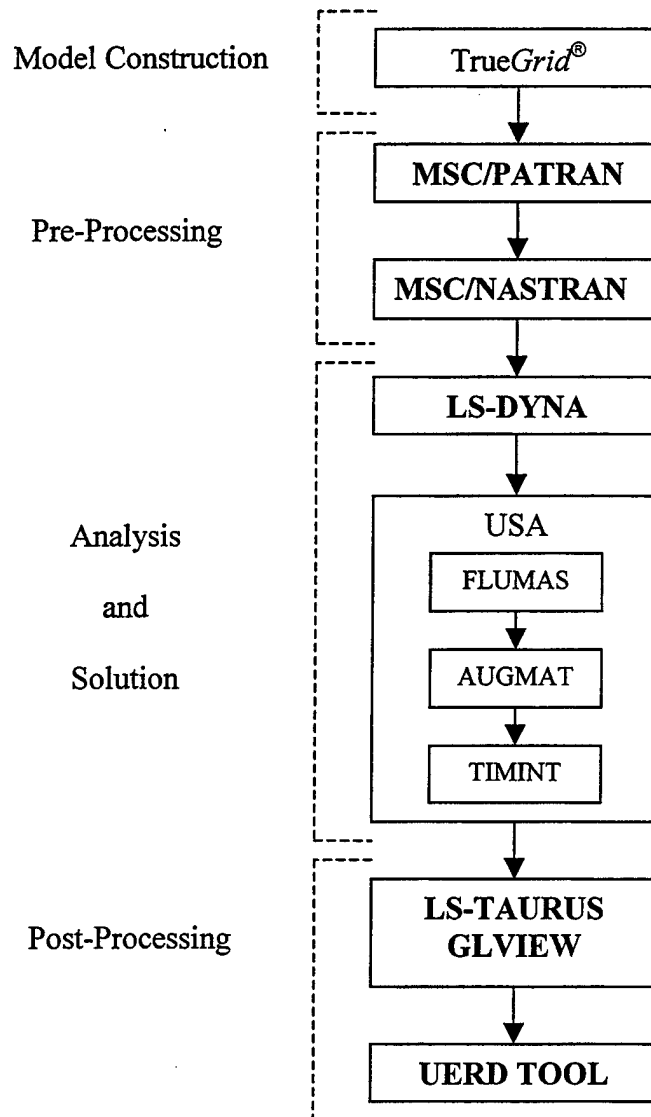
Figure 7. Flow Chart. Model Construction and Testing

17

A. MODEL CONSTRUCTION AND PRE-PROCESSING

1. Floating Shock Platform (FSP) Structural Model

The model of the Navy Standard Floating Shock Platform used for the heavyweight shock simulation was constructed using a finite element mesh generation program called True*Grid* [Ref. 6].

The model was developed using information detailed in the Military Specification for Shock Tests [Ref. 3]. The dimensions of the Navy Standard Floating Shock Platform are 288-in long, 192-in wide, 72-in deep on outside, and 36-in deep on the interior. For this application, it was possible to model only half of the platform due to symmetry. This was done to significantly reduce the computation time. This made the final model dimensions 144-in long, 192-in wide, 72-in deep on outside, and 36-in deep on the interior. The shell plating for the exterior of the modeled using thickness of ½ and 1-in steel having weight densities of 0.283, 0.317, and 0.340 lbf/in^3, Young's Modulus of 30x10^6 psi, and a Poisson's ratio of 0.3. The overall finite element mesh consists of 3669 nodes and 4116 quadrilateral (shell) elements. Table 1, Figures 8 and 9 show the model particulars. Figure 10 shows the overall finite element model.

Length	144-in
Beam	192-in
Depth (inside)	36-in
Depth (outside)	72-in
Design Waterline	36-in
Plating/Stiffener Material	40# S.T.S. and 20.4# HY-80 Steel
Plating/Stiffener Thickness	½-in and 1-in
No. of Nodes	3669
No. of Shell Elements	4116

Table 1. Model Specifications
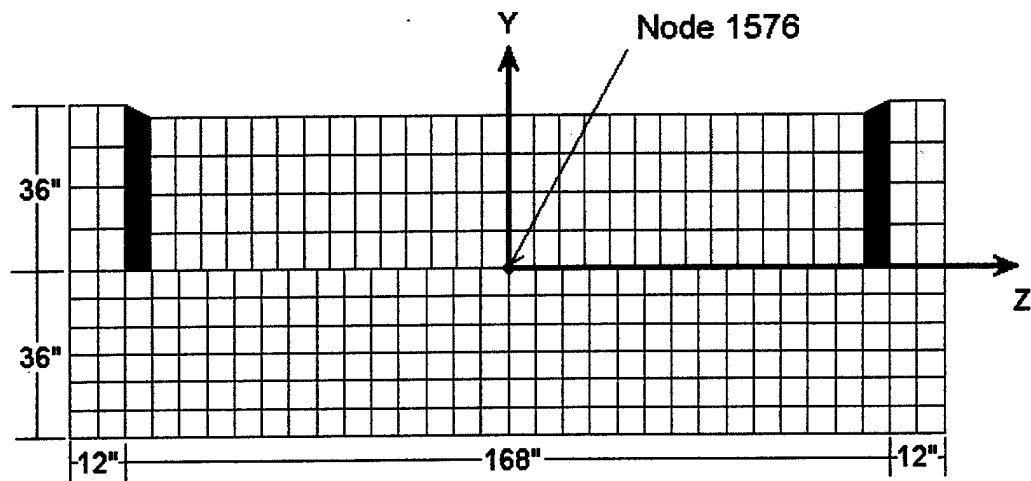
Front View
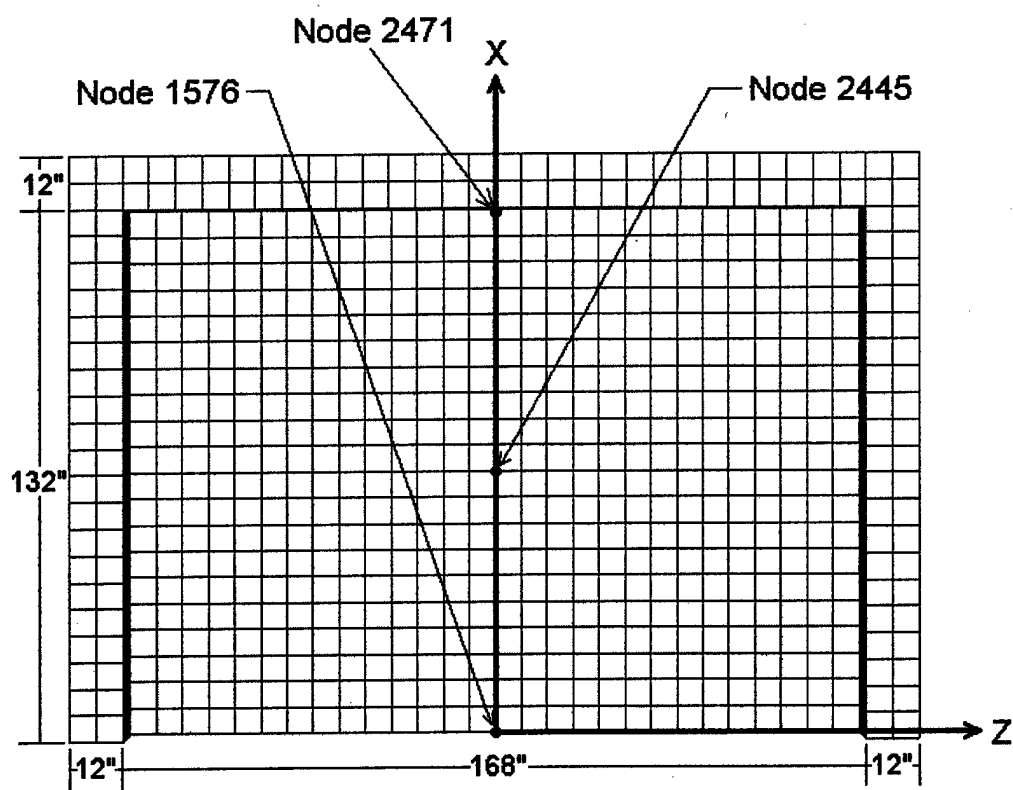
Top View

Figure 8. Model Specifications
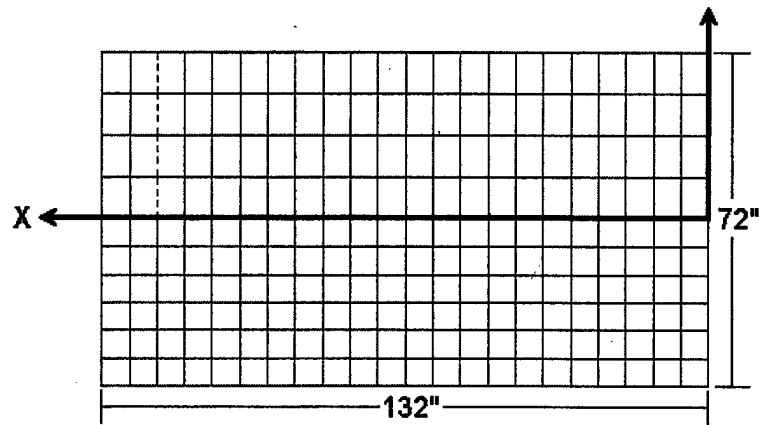
Side View

Figure 9. Model Specifications
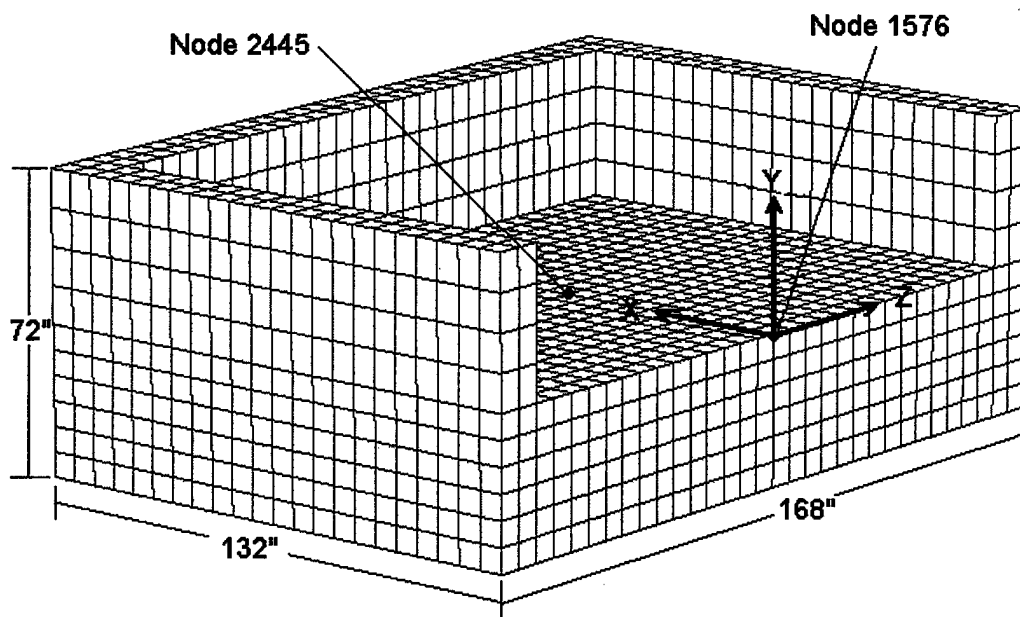
Figure 10. Finite Element Mesh

2. Fluid Modeling

Upon completion of the structural model, the next step was to design the fluid mesh. Element extrusion was performed using True*Grid*'s [Ref. 6] extrude command. Appendix D describes the use of this function in detail. The fluid mesh consists of 8-noded solid elements. LS-DYNA's Material Type 90 (acoustic pressure element) is used to model the pressure wave transmission properties of water [Ref 13]. Three different fluid size models were constructed for analysis. The extent (in the x and z directions) of the first fluid model was 672-in by 372-in, respectively. The depth of the mesh (under the FSP) was set to 108-in to ensure that the lower fluid boundary extended beyond the computed bulk cavitation zone (to be discussed later). This mesh (referred to as the full fluid size model) contains 57768 8-noded elements and 65808 total nodes and is shown in Figure 11. The size and complexity of a fluid mesh of this size requires extensive computational power to run a shock simulation. It is therefore beneficial to be able to reduce the size of this fluid mesh to save computational time.

The second fluid size model is a truncated or reduced size fluid mesh. The extent (in the x and z directions) of this mesh was set to 552-in by 276-in, respectively. The depth of this mesh (under the FSP) was set to 72-in, which places approximately half of the fluid mesh lower boundary outside the bulk cavitation zone. This mesh contains 47256 8-noded elements and 54636 total nodes and is shown in Figure 12. This fluid model will be referred to as the first fluid truncation.

The third fluid size model is a further truncation of the first fluid size model. It's extent (in the x and z directions) was set to 432-in by 228-in, respectively. The depth of this mesh (under the FSP) was set to 36-in, which places the entire fluid mesh within the bulk cavitation zone. This mesh contains 21010 8-noded elements and 27084 total nodes and is shown in Figure 13. This fluid model will be referred to as the second fluid truncation. A summary of each fluid size model is shown in Table 2.

An important aspect of a fluid mesh is the element size next to the structural mesh. For the cavitation analysis using the USA code, the critical element size is determined by the following equation [Ref. 15]:

$$\frac{2D\rho}{\rho_s t_s} \leq 5$$

Where ρ = density of water, D = thickness of the fluid element in the direction normal to the wetted surface of the structure, ρ_s = density of the submerged structure, and t_s = thickness of the submerged structure. It can be shown for this model that the critical element thickness, D, is 10 inches. The elements adjacent to this structural model were set a value less than this value of thickness.

	Full Fluid Size Model	First Truncation	Second Truncation
Length (x-dir)	372-in	276-in	228-in
Width (z-dir)	672-in	552-in	432-in
Depth (y-dir)	108-in	72-in	36-in
Number of Nodes	65808	54636	27084
Number of Elements	57768	47256	21010

Table 2. Summary of Finite Element Fluid Models
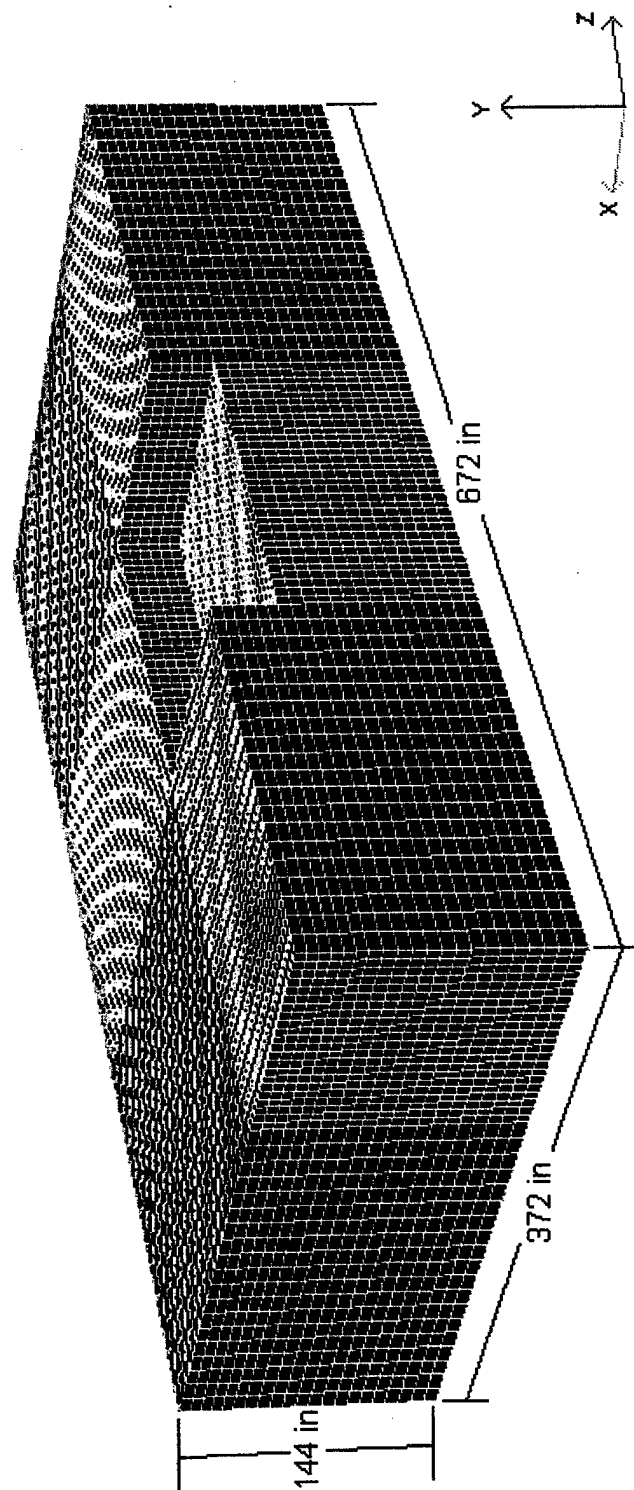
Figure 11. Full Fluid Size Model

23
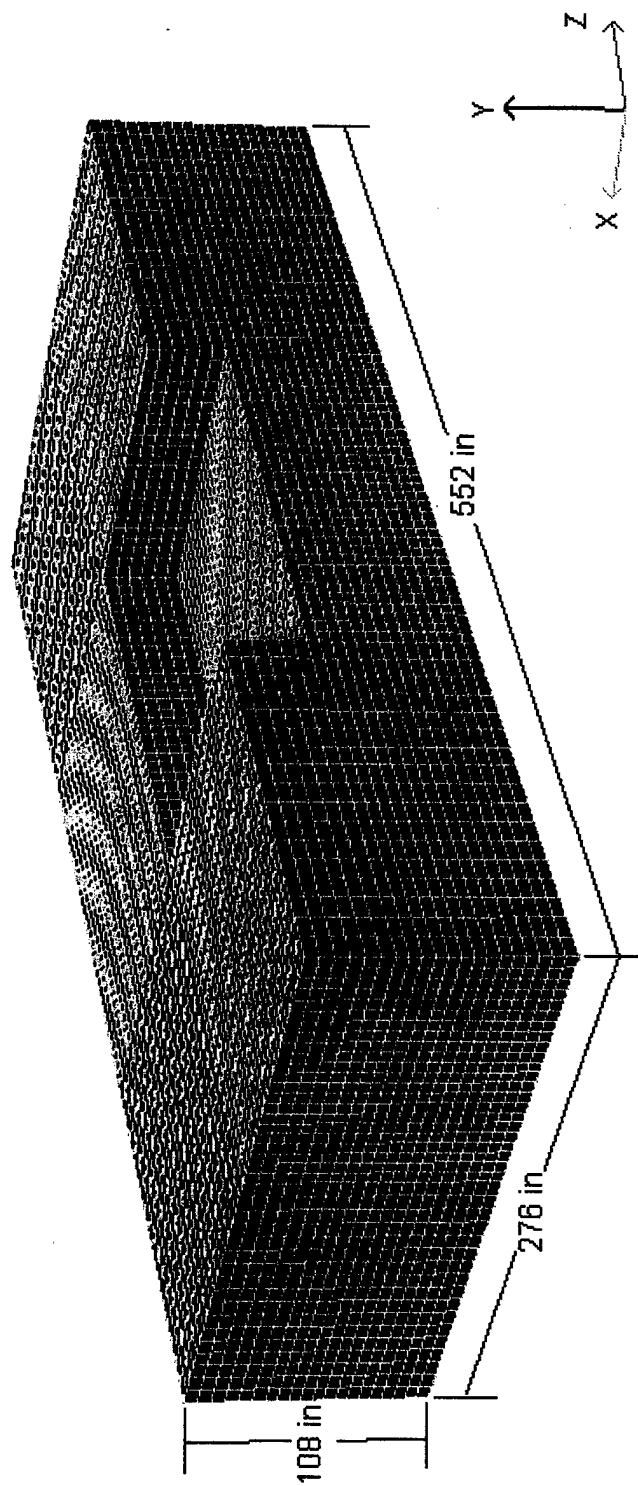
Figure 12. First Fluid Truncation
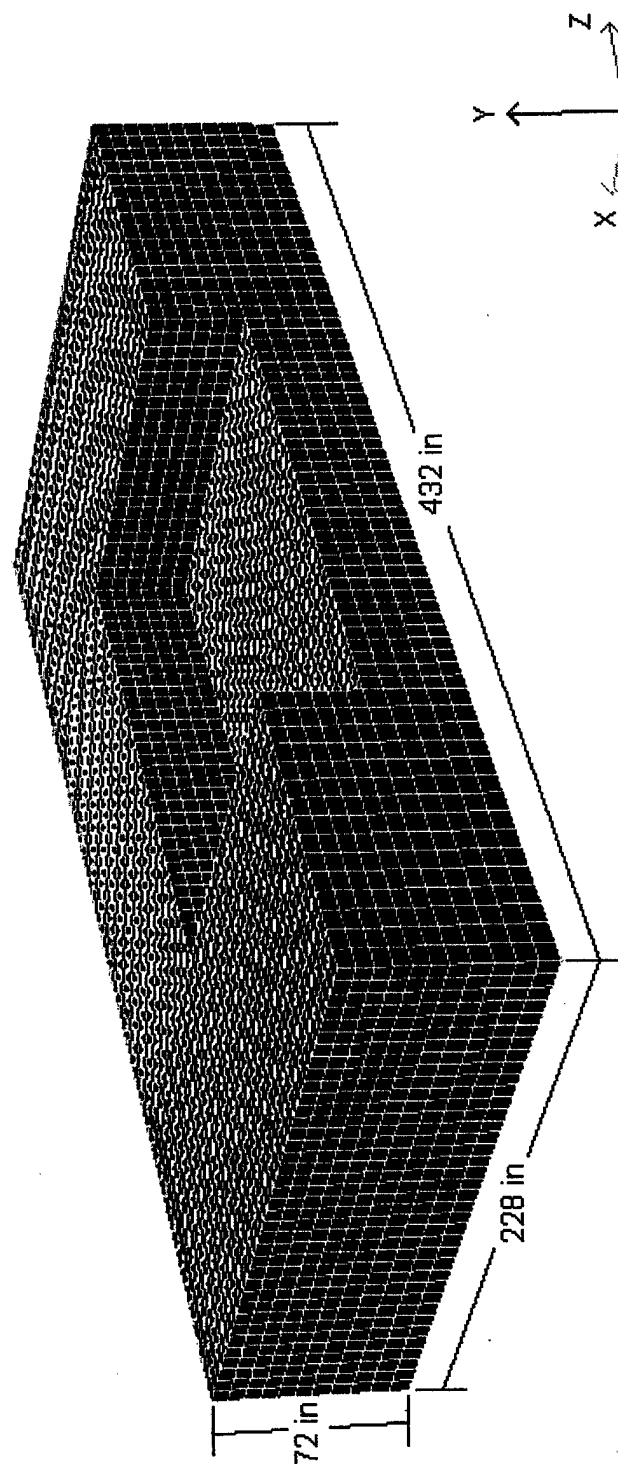
Figure 13. Second Fluid Truncation

B. ANALYSIS AND SOLUTION

1. Analysis Program Description

The finite element model must be translated into LS-DYNA keyword format in order to perform the analysis, since the LS-DYNA/USA coupled code is used. The USA code performs the majority of the work (formulation of the fluid-structure interaction matrices) and LS-DYNA is used to perform the time integration solution for the structure. LS-DYNA is a non-linear three-dimensional structural analysis code [Ref. 13]. The USA code consists of three main modules: FLUMAS, AUGMAT, and TIMINT.

FLUMAS is the first USA module required to be run. FLUMAS generates the fluid mass matrix for the submerged portion of the structure [Ref. 14]. The fluid mesh data, as well as the transformation coefficients that relate both the structural and fluid degrees of freedom on the wetted surface are generated, including the nodal weights for the fluid element pressure forces and the direction cosines for the normal pressure force. The fluid area matrix is diagonal and the fluid mass matrix is fully symmetric.

AUGMAT is the second module to be run. This module takes the data generated by the FLUMAS and initial LS-DYNA runs to construct specific constants and arrays utilized in the staggered solution procedure for the actual transient response analysis [Ref. 14]. The augmented interaction equations are formed from Equations (2.11) and (2.12). These two equations may be solved simultaneously at each time step, but this solution method can be very computationally expensive. The USA code uses a staggered solution procedure to achieve an efficient solution.

TIMINT performs the direct numerical time integration and also handles the computation of the UNDEX parameters, such as the shock wave pressure profile. The structural and fluid response equations are solved separately at each time step through the extrapolation of the coupling terms for the two systems. LS-DYNA is used to solve the structural equations and the TIMINT run solves the fluid equations. A result of using the staggered solution procedure mentioned previously, is that LS-DYNA and TIMINT can each have a different time step assigned. Although, the general practice is to use the same time step in both computations. Despite using an unconditionally stable solution

scheme, the TIMINT time step must be set small enough to accurately capture the fluid system response. Additionally, it should be mentioned that LS-DYNA uses a central-difference integration method, which is conditionally stable. The LS-DYNA time step must be less than or equal to the critical time step for the structural finite element mesh or numerical instability will result. Overall, this step of the solution procedure is the most time consuming and computationally expensive.

Appendix B provides example input decks for each of the three USA modules as well as an example LS-DYNA Keyword input deck.

2. Test Description

Two different charge location geometries were used in the shock simulation runs for this study. They are similar to charge locations specified for heavyweight shock testing of standard FSP's by Military Specifications for Shock Tests [Ref. 3].

A charge consisting of 60 lb. HBX-1 was chosen because of its specification in the same reference. One attack geometry placed the charge offset from the side of the FSP at the plane of symmetry (y-z plane) by 240-in. The charge depth is 288-in, with a standoff distance of 375-in. Figure 14 shows this attack geometry and Table 3 shows a summary of the UNDEX parameters of the explosion. The bulk cavitation zone was computed using the MATLAB program in Appendix A and is shown in Figure 15 along with the three fluid size mesh model boundaries. The second attack geometry consisted of the same 60 lb. HBX-1 charge, but placed directly under the FSP at the plane of symmetry (y-z plane) at a depth of 288-in. This resulted in a standoff distance of 252-in. Figure 16 shows this geometry and Table 4 summarizes the UNDEX parameters for this configuration. Once again, the bulk cavitation zone is shown in it's entirety and also on a larger scale which includes the three fluid size mesh model boundaries with respect to the FSP in Figure 17.
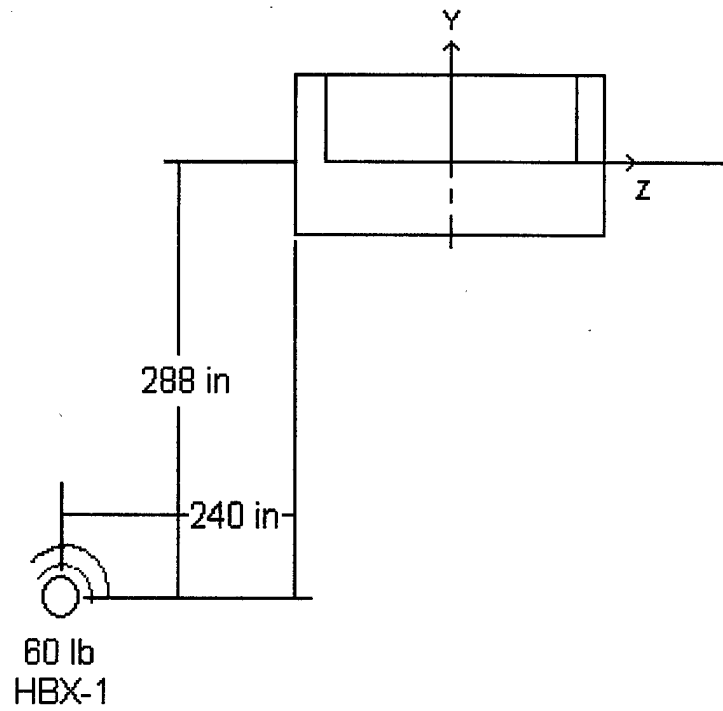
Figure 14. Offset Charge Test Geometry

Standoff Distance	375.0 in
P_{max}	2077 psi
θ	0.3662 msec
T	0.64 sec
A_{max}	172.60 in

Table 3. UNDEX Parameters for Offset Charge

Entire Bulk Cavitation Zone

FSP and Fluid Mesh Boundary Location in Bulk Cavitation Zone

Legend:
- Full Fluid Size Boundary
- 1st Fluid Truncation Boundary
- 2nd Fluid Truncation Boundary
- Bulk Cavitation Zone Boundary
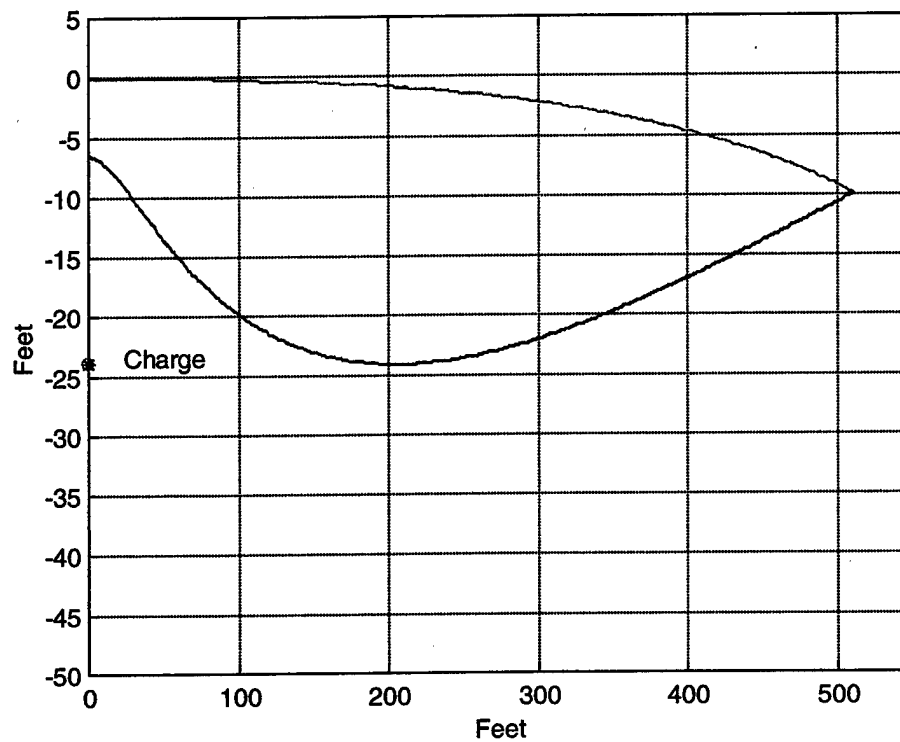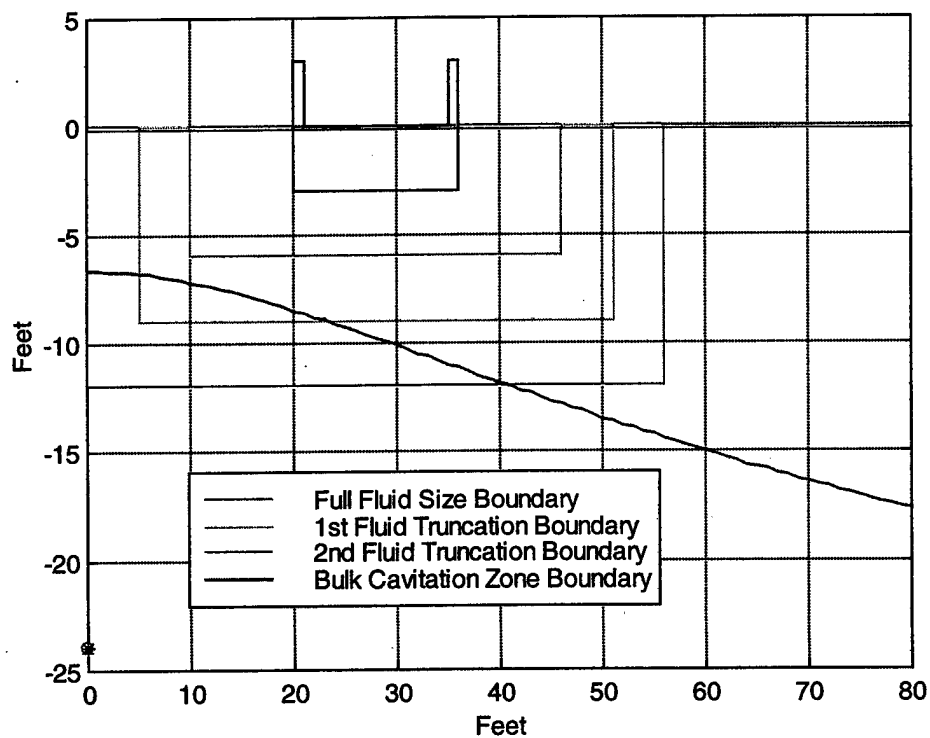
Figure 15. FSP in Bulk Cavitation Zone for a 60-lb. Charge (Offset) at 288-in

29
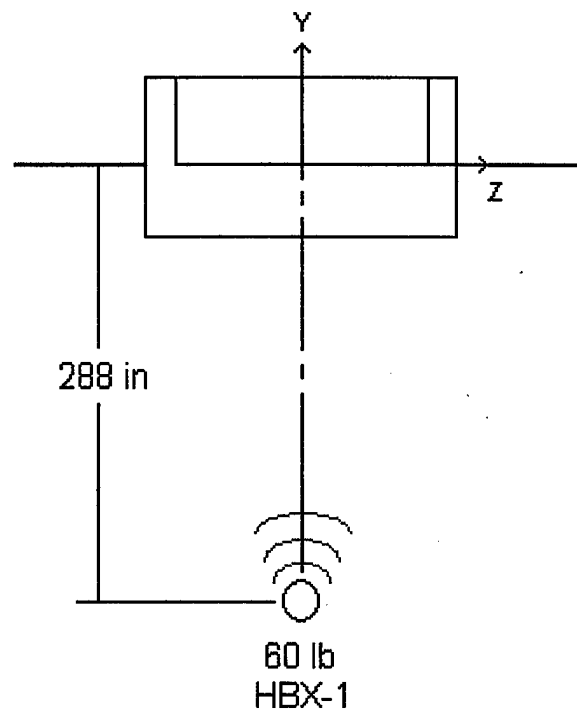
Figure 16. Charge Under FSP Test Geometry

Standoff Distance	252.0 in
P_{max}	3271 psi
θ	0.3320 msec
T	0.64 sec
A_{max}	172.60 in

Table 4. UNDEX Parameters for Charge Under FSP

Entire Bulk Cavitation Zone

FSP and Fluid Mesh Boundary Location in Bulk Cavitation Zone

Full Fluid Size Boundary
1st Fluid Truncation Boundary
2nd Fluid Truncation Boundary
Bulk Cavitation Zone Boundary
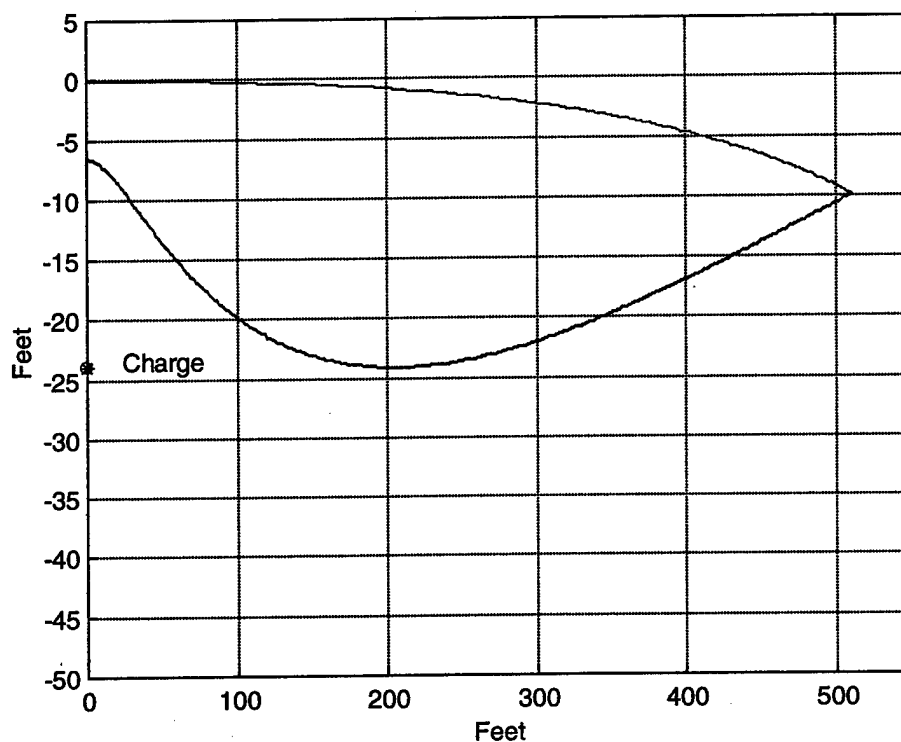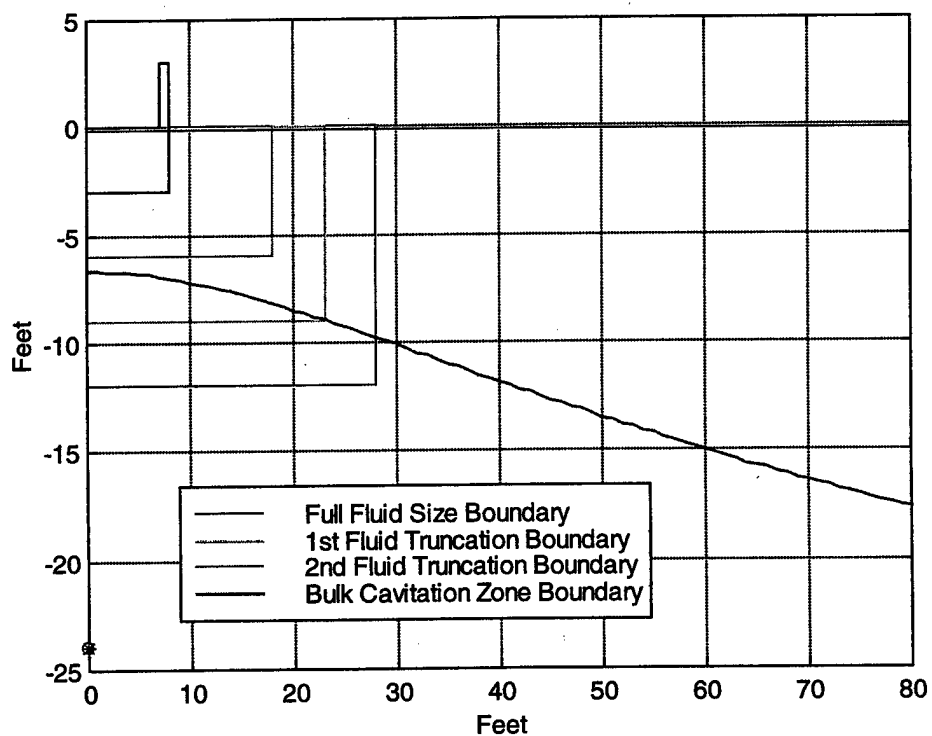
Figure 17. FSP in Bulk Cavitation Zone for a 20-lb Charge (Under) at 288-in

31

C.   POST-PROCESSING

The solution data is output into two formats for analysis: binary and ASCII. The binary data files created by the LS-DYNA/USA runs contain the model's finite element response information. LS-TAURUS [Ref 13] and Glview [Ref. 16] can both be used for three-dimensional response visualization. They provide powerful animation and image generation features, including the display of velocity, acceleration, and element pressure data. Additionally, both post-processing programs enable the user to observe the shock wave propagation through the fluid to the structure. LS-TAURUS has the capability of extracting ASCII solution data and writing it to a separate ASCII file for later evaluation. Appendix E provides some useful LS-TAURUS commands for model post-processing.

The ASCII data extracted by the LS-TAURUS post-processing program can be plotted and manipulated using UERD (Underwater Explosion Research Division) Tool software. This program is a PC-based plotting tool, which plots ASCII input files, provides standard graphing functions, as well as providing a variety of data manipulation features. These features include, but are not limited to curve integration and derivation of shock spectra.

IV. FSP SHOCK SIMULATION RESULTS

Three node points were used for comparison between the different fluid sized models in the simulation. The velocity response was analyzed at these nodes, specifically in the vertical (y) direction. These nodes are all located on the interior (floor) of the FSP. One node at the middle of the platform (closest to the symmetry plane), one at the interior end adjacent to the aft bulkhead, and one node ½ the distance between the other two nodes were chosen to provide a response at positions varying in stiffness. These nodes and their ID numbers are shown in Figures 8 and 10.

A.   CHARGE OFFSET FROM FSP

The first case examined was the geometry with the charge offset from the FSP. It was possible to run the simulation by placing the DAA boundary directly on the wetted surface of the structure, DAA boundary on the fluid mesh with cavitation flag off, or DAA boundary on the fluid mesh with the cavitation flag on. Results from a previous thesis [Ref. 17] concluded that the method of approximation the response by placing the DAA boundary on the fluid mesh with cavitation flag on is the most accurate. Therefore, this was the method chosen for this simulation. The simulation was run for all three fluid size mesh models in order to compare the effects of a truncated mesh on the response of the FSP.

The responses are plotted using the full fluid mesh size model results as a reference. Truncated fluid mesh size model responses are then plotted one at a time along with the full fluid mesh size response at each node for easier and clearer comparison. All simulations were run on an SGI Octane with two 195 MHz processors, 1.344 Gigabytes of RAM, and 23 Gigabytes of hard drive storage capacity. LS-DYNA version 940.2b and USA+ version 9801E were the simulation codes used.

For the full fluid mesh size model, a total of 3 hours was required for FLUMAS module to complete its computations. The AUGMAT module took 1 hour, 45 minutes to run, and the TIMINT module took 3 hours, 55 minutes to complete its calculations (with a time step of 2×10^{-5} seconds for 80 msec of data) for a total run time of 8 hours, 50

33

minutes. There was a considerable savings in computation time experienced for each truncated fluid mesh model. For the second fluid mesh truncated model, a total of 39 minutes was required for the FLUMAS module to complete its computations. The AUGMAT module took only 26 minutes to run, and the TIMINT module took just 1 hour, 29 minutes to complete its calculations (with the same time step and data duration) for a total run time of 2 hours, 34 minutes. The computation time was $^1/_3$ of the time necessary to run the full fluid mesh size model.

The vertical velocity response of the structure is what was expected. The velocity increases rapidly (approximately 5 to 6 msec) to a peak value and then rapidly decreases and increases in a series of steps until it settles down. The response does not settle out at a value of zero but instead slightly above that value due to rigid body motion of the structure. The reason for this behavior is from the fact that the incident shock wave impacts the structure with a very high pressure (close to 2100 psi) at approximately 5 to 6 msec from charge detonation and forces the structure rapidly upward. The structure is then quickly pulled downward as the shock wave reaches the free surface and a tensile wave is generated. This wave causes the pressure to decrease rapidly to zero psi, and cavitation occurs. Once cavitation occurs, the FSP is allowed to "break free" of the fluid, and the velocity of the structure again increases, albeit to a lower magnitude until the cavitating fluid contacts the structure pulling it downward again. This cycle continues past the point where the velocity of the structure is even negative momentarily to a value of just above zero, once again due to rigid body motion of the FSP.

The effect of fluid mesh truncation on the response of the structure is very slight. This can be seen in Figures 18 and 19. There is only a slight divergence after approximately 40 msec. Even with a fluid truncated model of approximately $^1/_8$ the size, the response is extremely accurate.

The athwartships (z-direction) velocity was also examined at the three structural nodes. Once again, there is fairly good correlation between the full fluid size meshed model and the first and second fluid truncated models.

The pressure at the middle and bottom of the fluid mesh underneath the FSP was examined. These pressure plots are included in Figures 22 and 23 and are element pressures taken directly below the structure. Cavitation can be seen to occur almost immediately underneath the model. Cavitation occurs almost continuously until approximately 40 msec, when the effects of the initial shock wave and rarefaction waves have subsided allowing the fluid pressure to again reach a state above zero. This response correlates well with the velocity response seen in the FSP in Figures 18 through 21. Additionally, pressure profiles at the depths examined were expected to show cavitation for a large duration (after the initial shock wave passed) since these depths fall within the bulk cavitation zone computed and shown in Figure 15.

It should be pointed out that the magnitude of the initial shock wave pressure shown in the pressure profile plots in Figures 22 and 23 was far below what was expected (approximately half of the expected value). This can be explained by the fact that the decay constant of the incident shock wave has a value of 0.3662 msec as shown in Table 3. With a decay constant this high, the pressure wave will decay over a distance of approximately 21.75 inches (assuming a fluid sound speed of 4952.4 ft/sec). The fluid mesh refinement used for this study has a diagonal distance across elements of 14 inches. This distance allows the incident shock wave pressure to decay to value less than half of its actual pressure before it is imparted on the element adjacent to it. This is expected to cause an deviance in fluid pressure of approximately 50 percent when the value is extracted from the LS-DYNA/USA program run data files. Indeed, this is what is seen in Figures 22 and 23.

This difference between program calculated values of pressure and actual expected values was not considered a major concern, since the majority of the FSP's response is developed from the fluid particle's impulse imparted on the structure and not the peak pressure of the incident wave on it. Also, for this study, the interest was more toward the comparison of the FSP's structural response and fluid pressure profile when a fluid mesh of a given size was truncated.

A solution to resolve the fluid pressure decay across the fluid mesh element is to reduce the size of the element used. For this case, when the decay constant is high, the fluid element dimensions must be reduced to a size, which does not allow a significant reduction in peak pressure across the element during program integration.

Node 1576
Vertical Velocity

Full Fluid Size Model ——— First Fluid Truncation

Node 2445
Vertical Velocity

Full Fluid Size Model ——— First Fluid Truncation

Node 2471
Vertical Velocity

Full Fluid Size Model ——— First Fluid Truncation
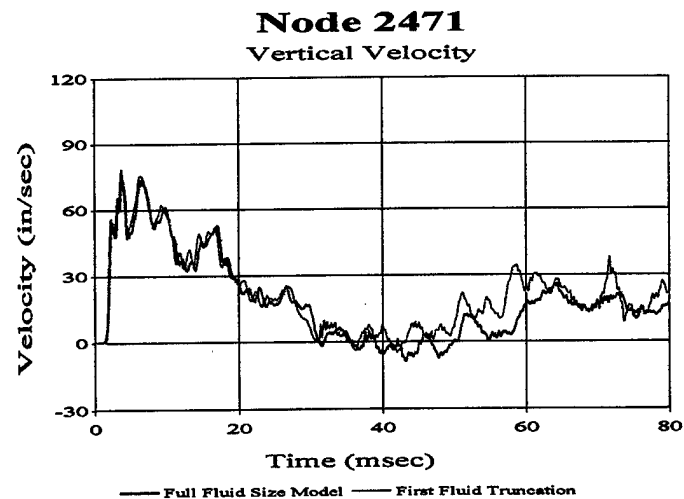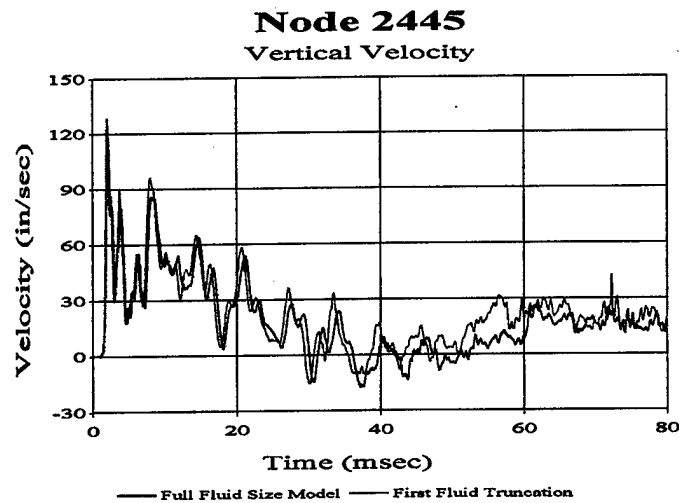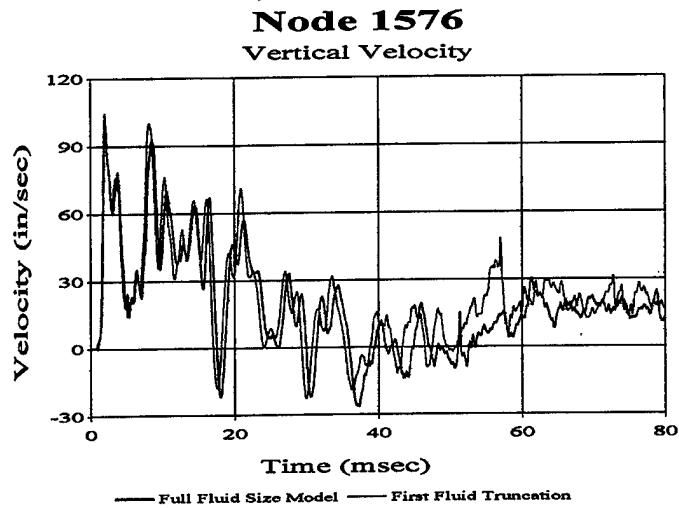
Figure 18. Vertical Velocity Response w/Charge Offset from FSP

37

Node 1576
Vertical Velocity

Full Fluid Size Model   Second Fluid Truncation

Node 2445
Vertical Velocity

Node 2471
Vertical Velocity

Full Fluid Size Model   Second Fluid Truncation
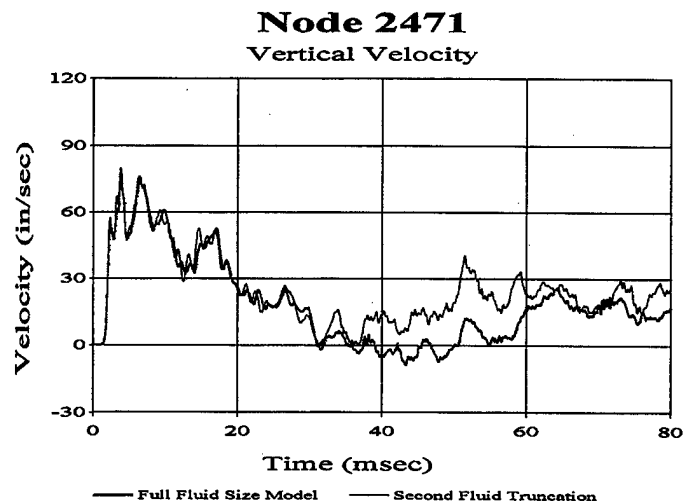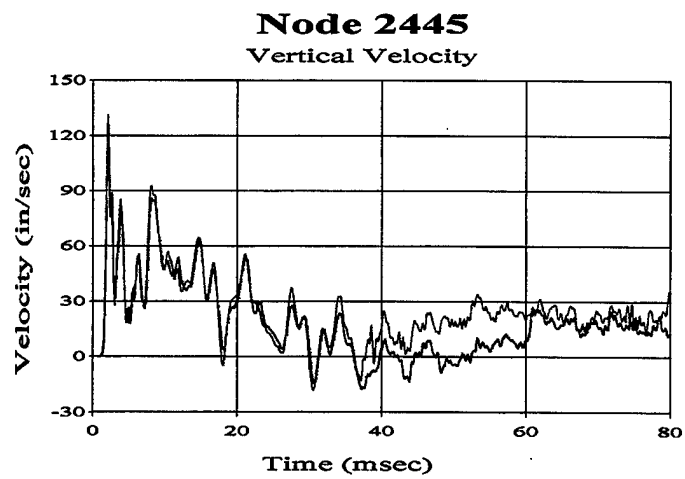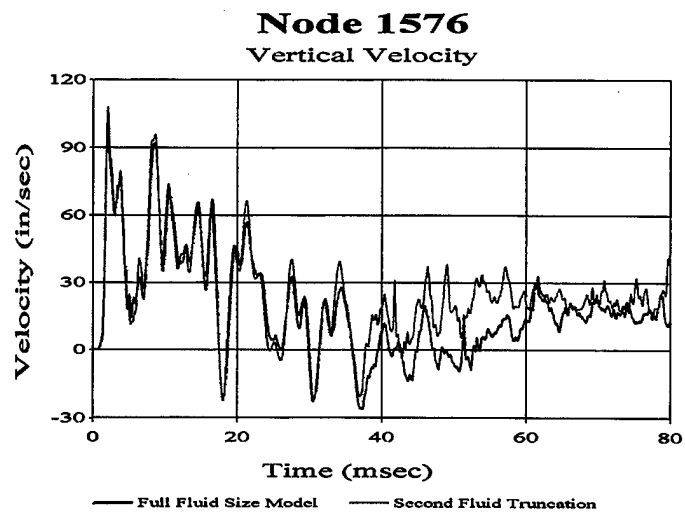
Figure 19. Vertical Velocity Response w/Charge Offset from FSP

Node 1576
Athwartships Velocity (Z-Dir)

Full Fluid Size Model ——— First Fluid Truncation

Node 2445
Athwartships Velocity (Z-Dir)

Full Fluid Size Model ——— First Fluid Truncation

Node 2471
Athwartships Velocity (Z-Dir)

Full Fluid Size Model ——— First Fluid Truncation
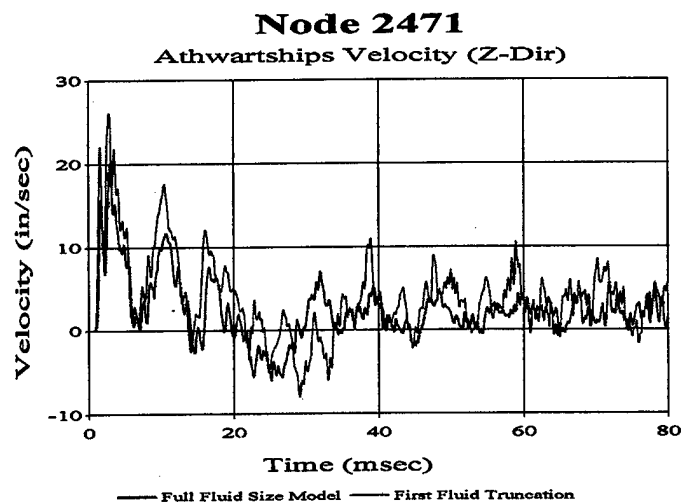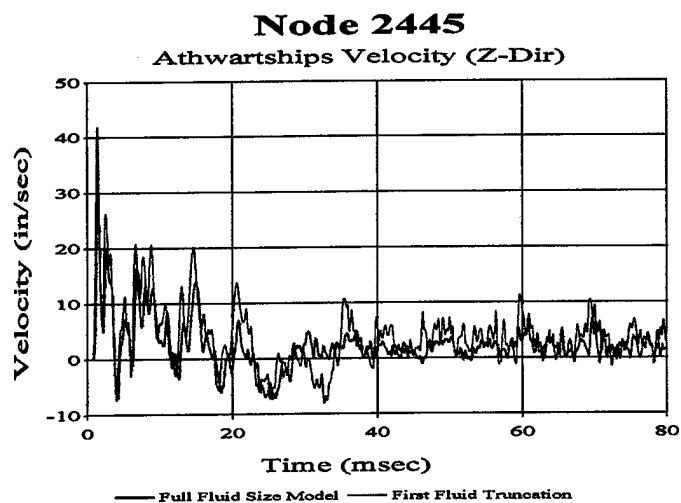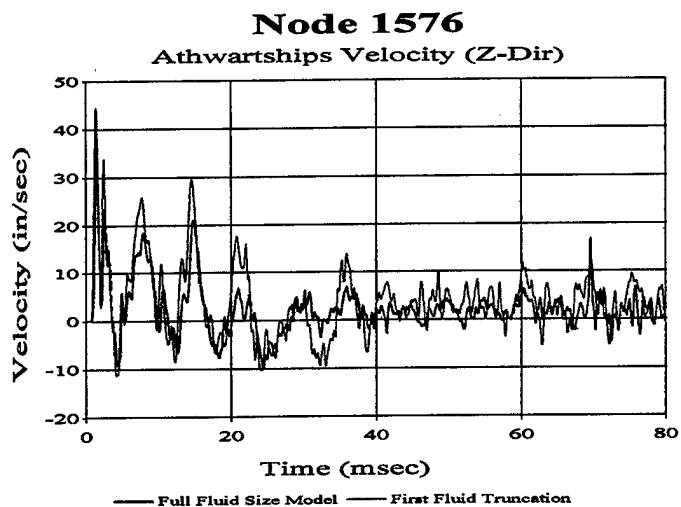
Figure 20. Athwartships (Z-Dir) Velocity Response w/Charge Offset from FSP

39
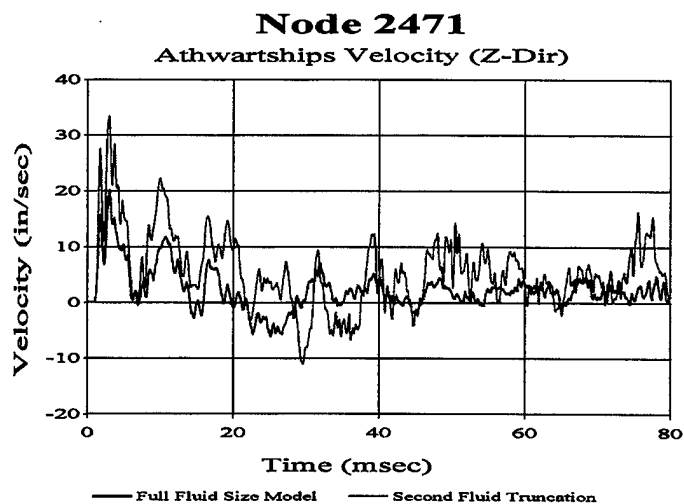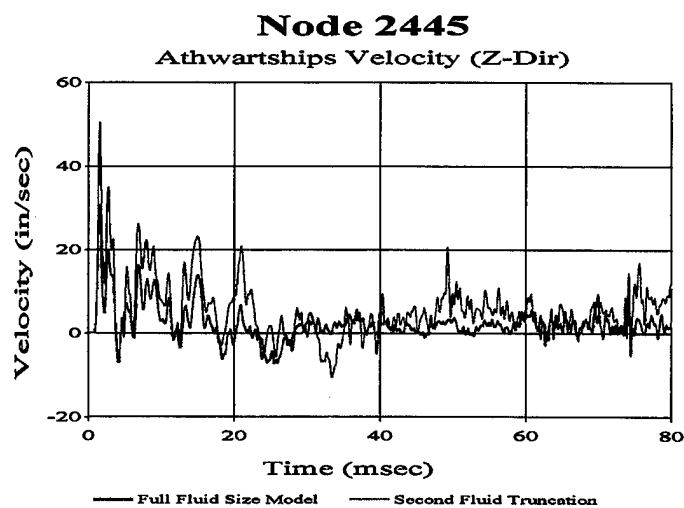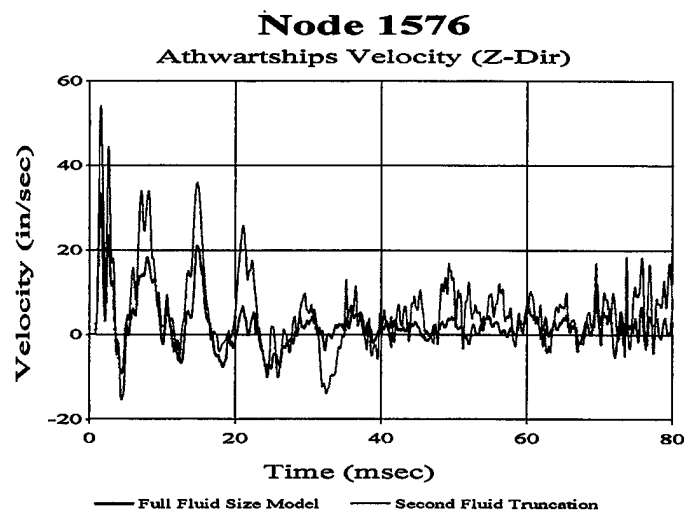
Figure 21. Athwartships (Z-Dir) Velocity Response w/Charge Offset from FSP

Middle of Fluid Mesh

36" below FSP

Full Fluid Size Model ——— First Fluid Truncation
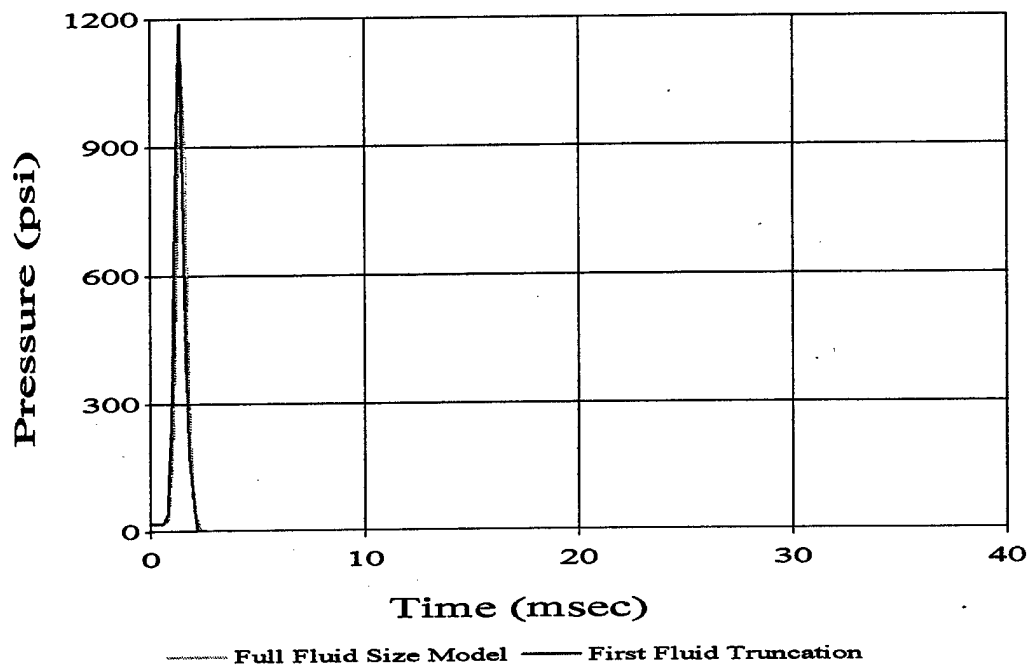
Bottom of Fluid Mesh

67" below FSP

Full Fluid Size Model ——— First Fluid Truncation
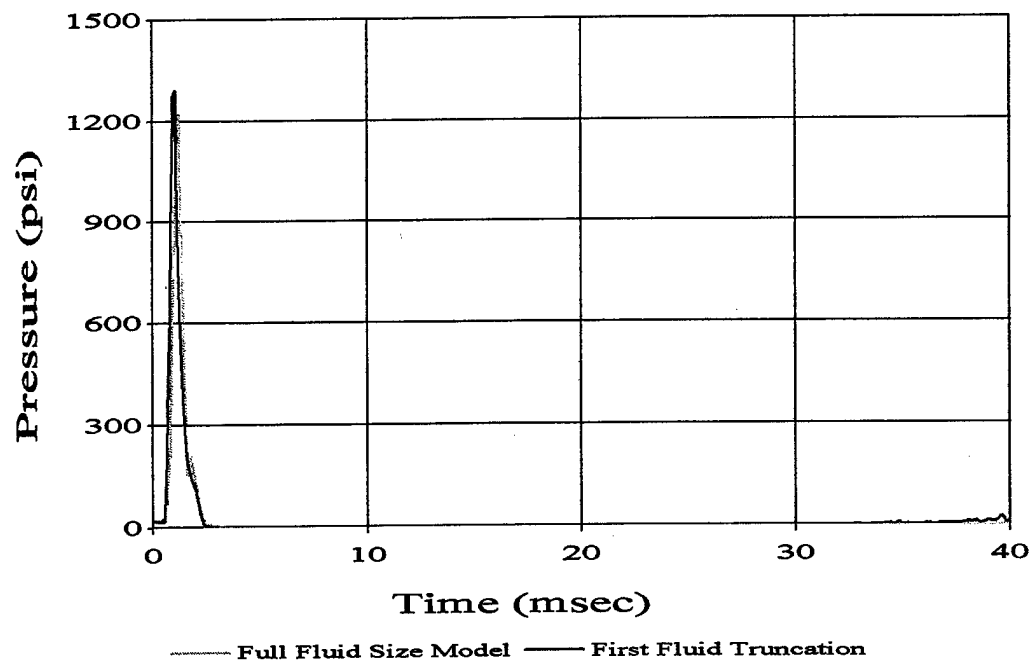
Figure 22. Fluid Mesh Pressure Profiles w/Charge Offset from FSP

41

Middle of Fluid Mesh
14" below FSP

Full Fluid Size Model   Second Fluid Truncation

Bottom of Fluid Mesh
29" below FSP

Full Fluid Size Model   Second Fluid Truncation
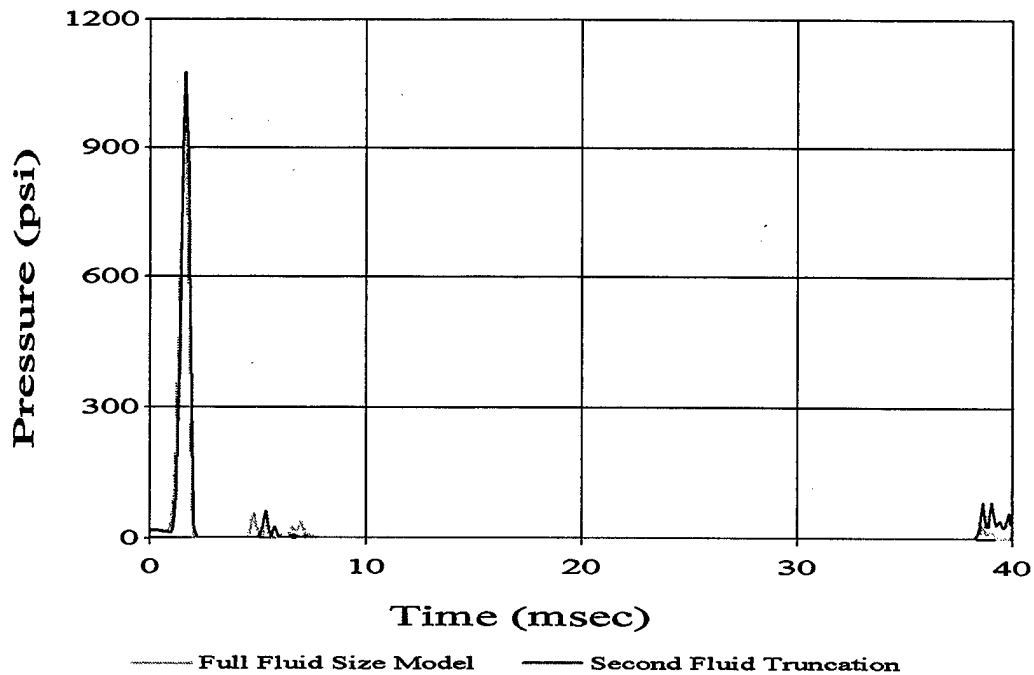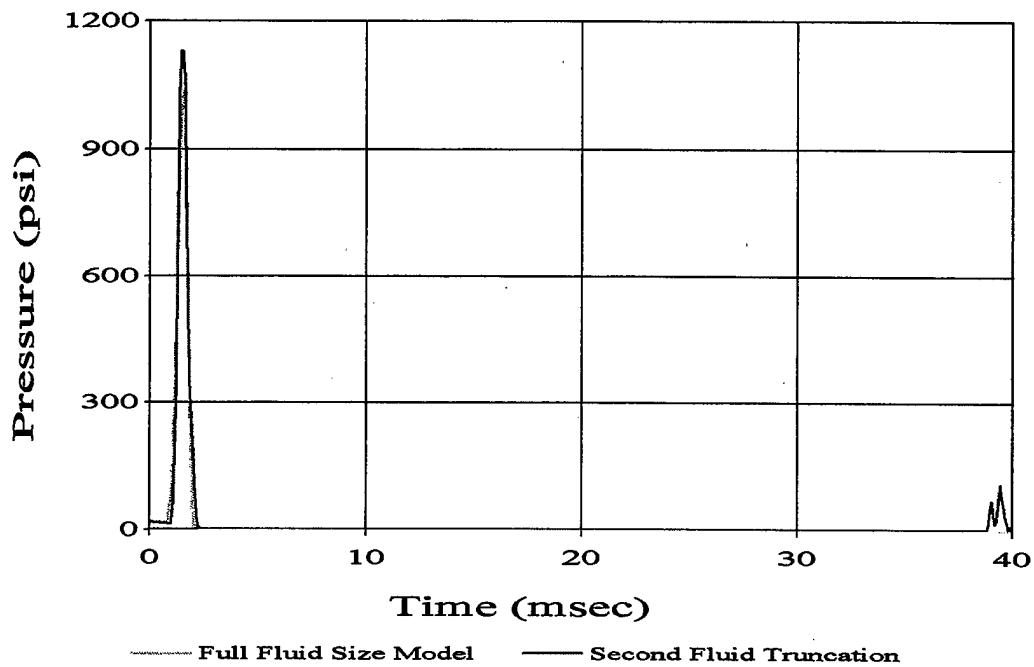
Figure 23. Fluid Mesh Pressure Profiles w/Charge Offset from FSP

42

B. CHARGE UNDER FSP

The shock simulations were also run and compared for the geometry with the charge placed directly under the FSP along the plane of symmetry (y-z plane). The same combination of runs was conducted as for the charge offset from the FSP. The resulting responses are quite similar in nature to those described in section A of this chapter.

Vertical velocity response profiles are plotted in Figures 24 and 25. Once again, the velocity response increases rapidly to a peak value and then rapidly decreases and increases in a series of steps until it settles down. The response for this case takes slightly longer to reach a somewhat steady state because the magnitude of the incident pressure wave is a larger value (3271, vice 2077 psi). However, as in the offset charge geometry, the structural velocity settles out to a value above zero because of the rigid body motion of the FSP.

The effect of the fluid mesh truncation on the response of the structure is slight as in the previous geometry. The slight divergence encountered occurs after approximately 60 msec. However, even with the extent of truncation between the full fluid size model and the second fluid truncated model, the deviance is not large.

Again, pressure at the middle and bottom the fluid mesh underneath the FSP was compared. These pressure profile plots are shown in Figures 26 and 27. Cavitation occurs as expected, almost immediately (following the initial shock wave pressure pulse). In this geometry, it can be more readily seen that the pressure deeper in the fluid mesh experiences cavitation for a much shorter duration of time. In fact, cavitation subsides within approximately 20 msec at depth of 29-in. as seen in Figure 27. Cavitation does indeed occur, as predicted, since this depth falls within the computed bulk cavitation zone plotted in Figure 17. The bulk cavitation zone depth directly under the FSP was computed to a depth of approximately 72 inches. Therefore, cavitation is expected to occur in each of the pressure profile comparison plots. The deeper pressure profile plot comparison at 62 inches below the FSP shown in Figure 26 indicates cavitation occurs for a much shorter duration (approximately 10 msec) as expected.

43

As was previously discussed in section A of this chapter, the magnitude of the initial shock wave pressure shown in Figures 26 and 27 was much less than expected. The cause for the deviance and solution is the same as was discussed previously. Once again, because the basis of this study was structural response comparison when a given fluid size mesh is truncated, this was not seen as a major concern, but one, which must still be addressed, as was done here.

Node 1576
Vertical Velocity

Full Fluid Size Model ——— First Fluid Truncation

Node 2445
Vertical Velocity

Full Fluid Size Model ——— First Fluid Truncation

Node 2471
Vertical Velocity

Full Fluid Size Model ——— First Fluid Truncation
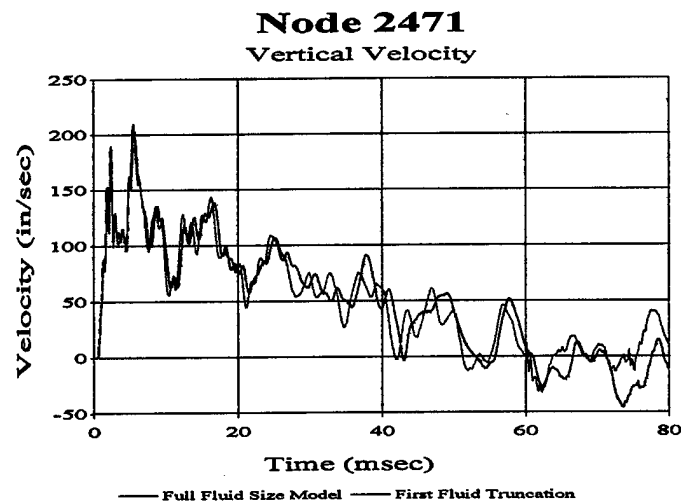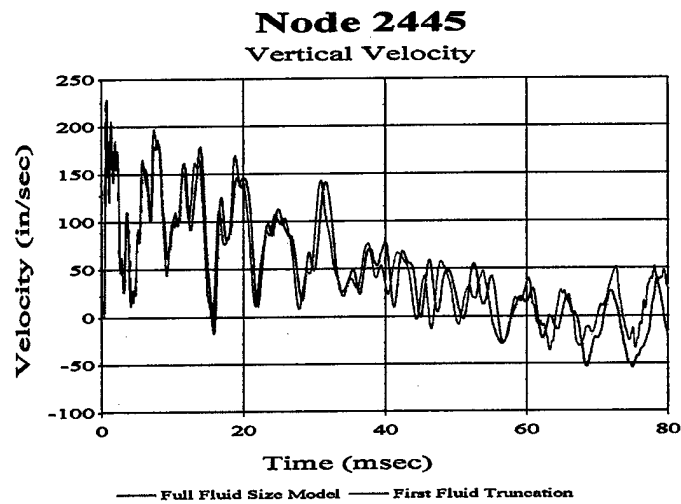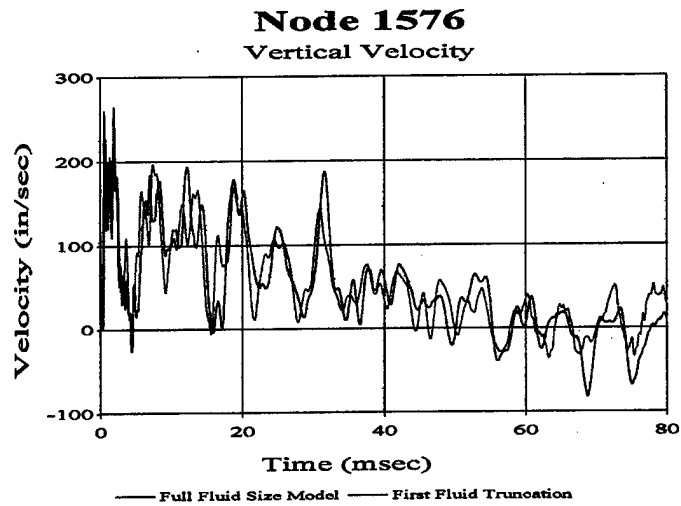
Figure 24. Vertical Velocity Response w/Charge Under FSP

45

Node 1576
Vertical Velocity

Full Fluid Size Model ———— Second Fluid Truncation

Node 2445
Vertical Velocity

Full Fluid Size Model ———— Second Fluid Truncation

Node 2471
Vertical Velocity

Full Fluid Size Model ———— Second Fluid Truncation
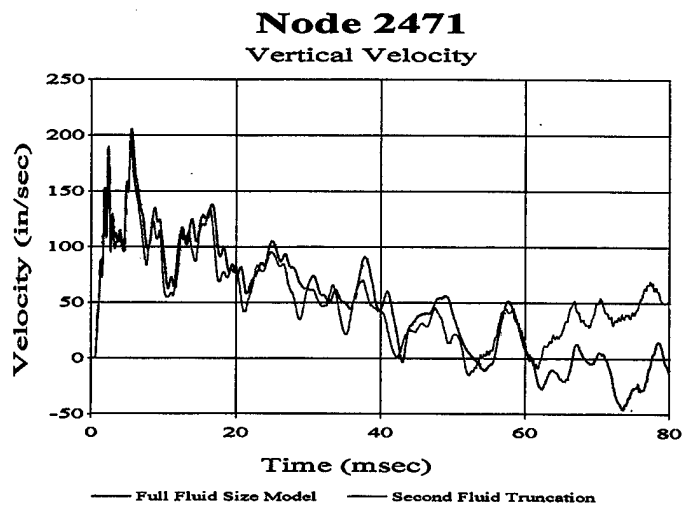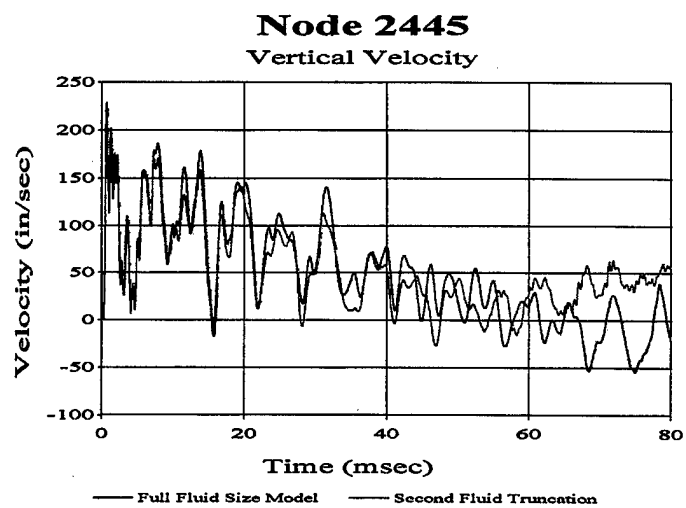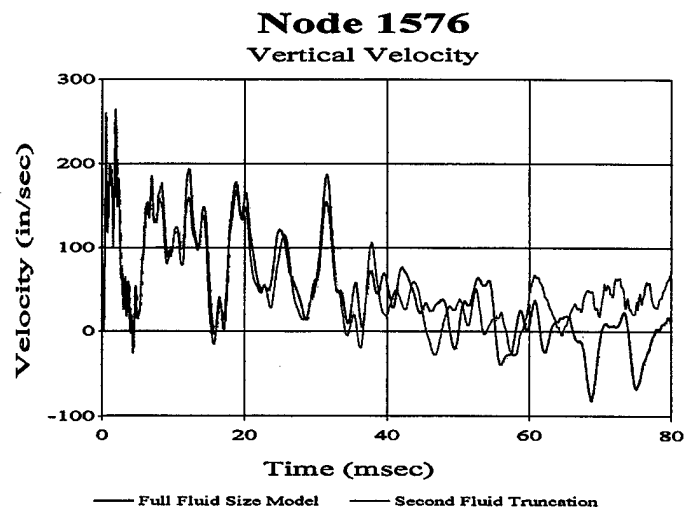
Figure 25. Vertical Velocity Response w/Charge Under FSP

46

Middle of Fluid Mesh
21" Below FSP

Full Fluid Size Model —— First Fluid truncation
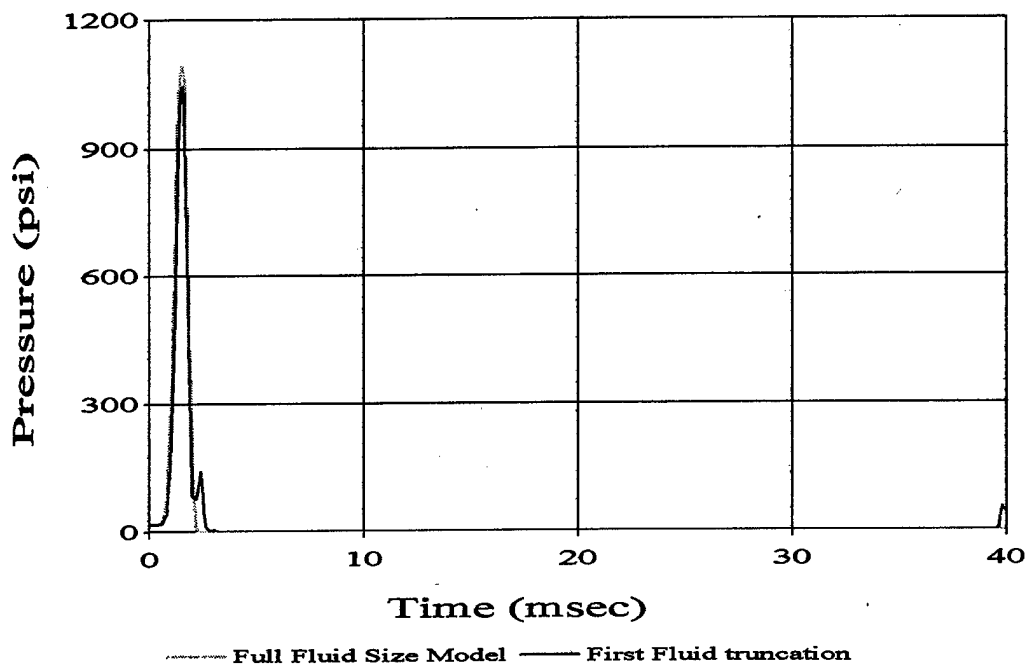
Bottom of Fluid Mesh
62" Below FSP

Full Fluid Size Model —— First Fluid Truncation
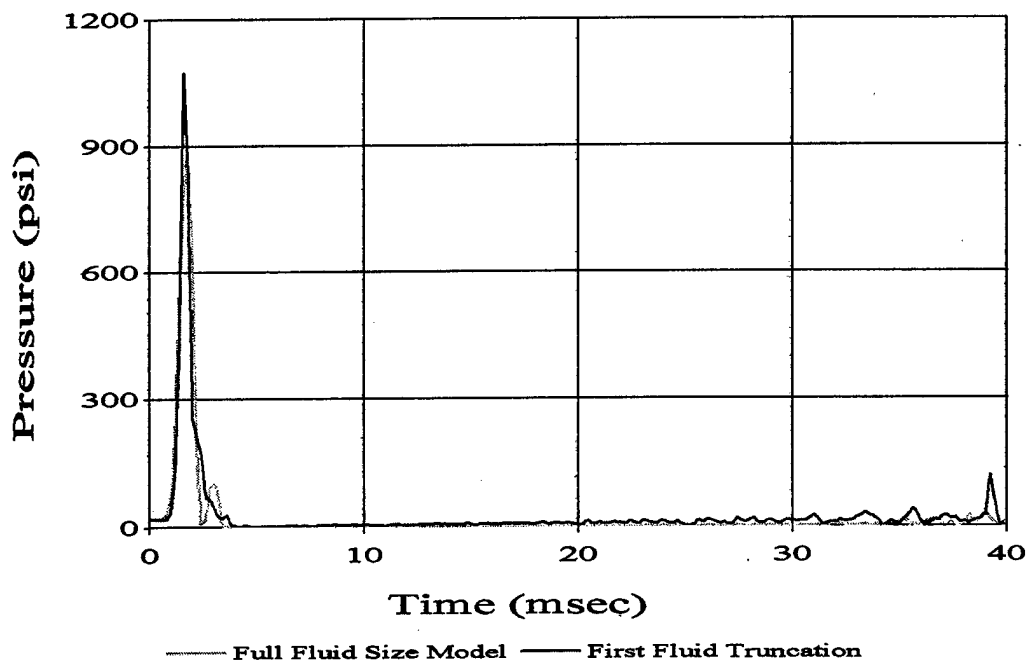
Figure 26. Fluid Mesh Pressure Profiles w/Charge Under FSP

47

Middle of Fluid Mesh
12" below bottom

Full Fluid Size Model — Second Fluid Truncation

Bottom of Fluid Mesh
29" Below FSP

Full Fluid Size Model — Second Fluid Truncation
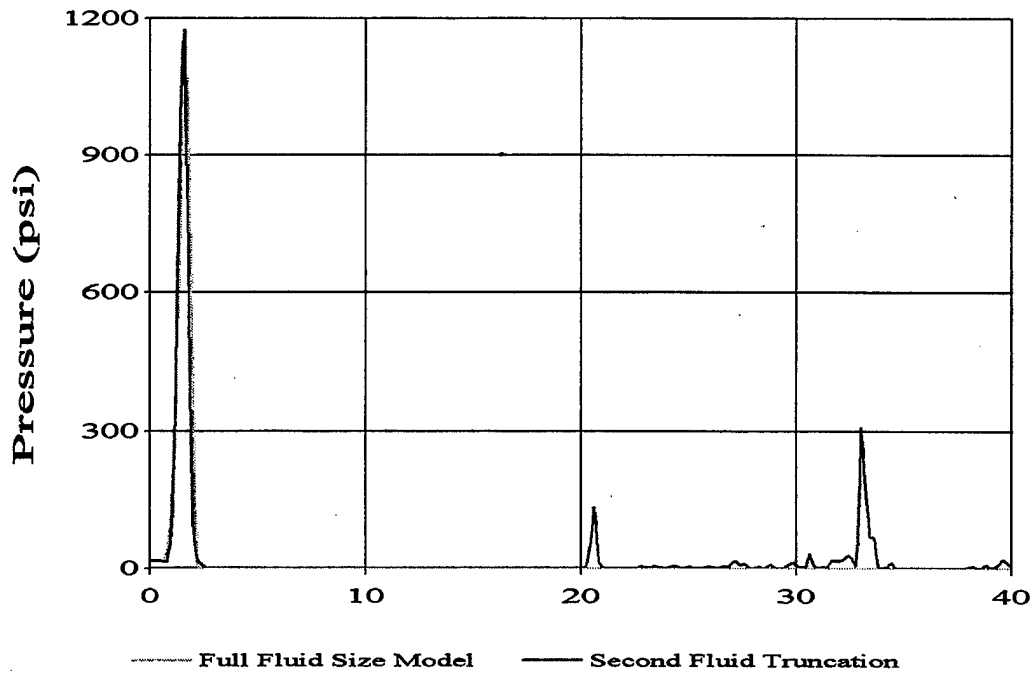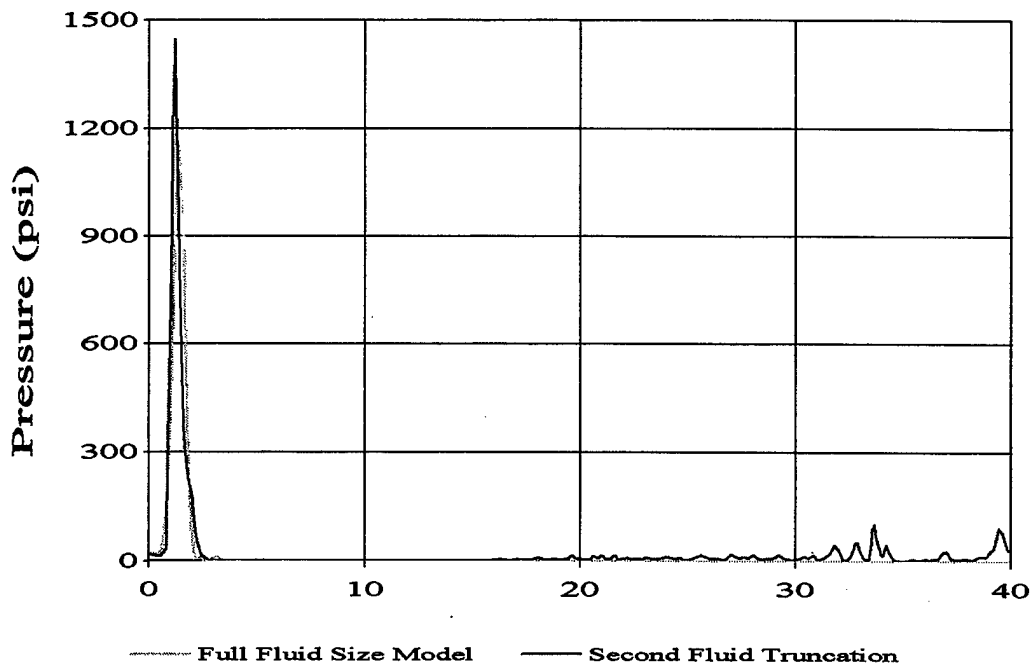
Figure 27. Fluid Mesh Pressure Profiles w/Charge Under FSP

V. CONCLUSIONS AND RECOMMENDATIONS

This thesis investigated the effect of reducing or truncating the fluid mesh in a fluid-structure finite element model on the accuracy of a FSP's response to an underwater explosion. There is no question that when practical, a fluid mesh size large enough to capture the extent of a computed bulk cavitation zone should be used to obtain the most accurate structural response possible.

However, when computer extent and computational time is an issue, as is increasingly more probable as finite element models become more complex, it is of high importance to develop a means to obtain accurate results while minimizing computational effort. Fluid mesh truncation was explored as a means to reduce the computation time of LS-DYNA/USA coupled code to calculate a solution for the structural response to an underwater explosion event.

The structural velocity response results of the FSP with truncated fluid size models agreed closely with the response obtained by modeling a larger size fluid mesh. The responses were not only in close agreement with the other model runs, but the values obtained agreed with predicted behavior based on the physics of the situation. Slight deviation in model results may be attributed to minor differences in program input parameters. In any case, fluid mesh truncation clearly demonstrated that the effects of fluid mesh truncation are very slight and that it is a viable option for reducing the computation time of solving otherwise large finite element fluid-structure models.

It is recommended that additional studies be conducted to more fully examine the effects of fluid mesh truncation in underwater explosion simulations. Specifically, the following areas should be studied:

1. Vary the fluid size adjacent to the FSP to determine if there is a minimum amount of fluid required for modeling to obtain accurate structural response.

2. Vary the fluid element size to examine the effect on fluid element pressure accuracy with expected results.

49

3. Model selected equipment mounted on FSP in order to compare live fire testing results with computed results.

4. Apply fluid mesh truncation to more complex models, such as U.S. Navy Warships, to investigate the accuracy of the model response to known live fire testing data.

APPENDIX A. BULK CAVITATION PROGRAM

The following program code calculates the bulk cavitation zone by solving Equations (2.22) and (2.23). The code is written for MATLAB Version 5.2 [Ref. 12].

```
% Bulk Cavitation Program Using HBX-1 as Charge Type
% Written by: James R. Smith
% MATLAB Version 5.2

% This program is used to compute both the upper and lower cavitation
% boundaries for a given input of HBX-1 charge weight and charge depth.
% This program can easily be modified to handle other explosive types.
% However, shock wave parameters (K1,K2,A1,A2) would need to be
% updated. "Standard" atm pressure, seawater specific weight and speed
% of sound are used. These values can be changed to achieve desired
% accuracy for a particular problem. This program is set up as is to
% handle cavitation boundaries out to 2200ft (x) and to a depth of 50ft
% (y). These parameters can be changed as required.

% Program Start

clear all;

% Defining constants

Pa = 14.7;          % atmospheric pressure (psi)
C = 4900;           % acoustic velocity (ft/s) @ 64.4F (18C)
gamma = 0.037031;   % weight density of seawater @ 68F and 1 atm (lbm/in^3)

K1 = 22347.6;       % Shock Wave
K2 = 0.056;         % Parameters
A1 = 1.144;         % explosive type
A2 = -0.247;        % specific

% Prompting user to enter charge weight and depth
disp(' ')
W = input('Enter the charge weight of HBX-1 in lbf: ');
D = input('Enter the charge depth in feet: ');

W_text = num2str(W);
D_text = num2str(D);

disp(' ')
disp(['Calculating the bulk cavitation zone for a ',W_text,'lb HBX-1
explosion'])
disp(['at a depth of ',D_text,' feet'])
disp(' ')

% Beginning calculation of upper and lower cavitation boundaries

% theta = decay constant
% x = horizontal distance
```

```
% y = vertical distance
% r1,R = standoff distance from charge to point
% r2 = standoff distance from image charge to point
% Pi = incident shock wave pressure at tc

data_u = []; % Creating a matrix to store upper boundary data
data_l = []; % Creating a matrix to store lower boundary data

% Calculating Upper Boundary
for x = 0:600
        for y = 0:0.1:50
                r1 = sqrt((D-y)^2+x^2);
                r2 = sqrt((D+y)^2+x^2);
                theta = K2*W^(1/3)*(W^(1/3)/r1)^A2/1000;
                F =(K1*(W^(1/3)/r1)^A1*exp(-(r2- r1)/(C*theta)))
                +Pa+(gamma*y*12)-(K1*(W^(1/3)/r2)^A1);

                if F <= 0 % Testing for cavitation
                        data_u = [data_u; F x -(y)];
                break,end
        end
end

% Calculating lower boundary
for x = 0:(length(data_u)-1)
        for y = 0:0.1:50
                r1 = sqrt((D-y)^2+x^2);
                r2 = sqrt((D+y)^2+x^2);
                theta = K2*W^(1/3)*(W^(1/3)/r1)^A2/1000;
                Pi = K1*(W^(1/3)/r1)^A1*exp(-(r2-r1)/(C*theta));
                G = -(Pi/(C*theta))*(1+(((r2-
                (2*D*(D+y)/r2))/r1)*(((A2*r2)/r1)-A2-1)))-((A1*Pi)/r1^2)*(r2-
                2*D*((D+y)/r2))+
                (gamma*12)*((D+y)/r2)+(A1/r2)*(Pi+Pa+(gamma*y*12));

                if G >= 0 % Testing for cavitation
                        data_l = [data_l; G x -(y)];
                break,end
        end
end

%Truncating cavitation boundaries at intersection

index_u = find(data_u(:,3)<data_l(:,3));
index_l = find(data_l(:,3)>data_u(:,3));
data_u(index_u,:)=[];
data_l(index_l,:)=[];

%Plotting cavitation boundaries
plot(data_l(:,2),data_l(:,3),data_u(:,2),data_u(:,3)); grid;
axis([0,550,-50,5]);
title(['Cavitation Zone for a ',W_text,' lb HBX-1 Charge at a Depth of
',D_text,' feet']);
xlabel('Feet'); ylabel('Feet');
```

APPENDIX B. USA/LS-DYNA INPUT DECKS

This section of this appendix provides example USA input decks for each of the three USA modules: FLUMAS, AUGMAT, and TIMINT. Reference 18 provides information concerning the various input deck variables.

An example LS-DYNA KEYWORD input deck is included also from the full fluid size model. Only the first line or two of each card is included. Reference 16 provides information as to the meaning of each field on the cards.

USA INPUT DECKS:

```
FLUMAS DATA FOR FSP
flunam geonam strnam daanam          $ FLUNAM GEONAM GRDNAM
DAANAM
F F F T                              $ PRTGMT PRTTRN PRTAMF
CALCAM
F F T F                              $ EIGMAF TWODIM HAFMOD
QUAMOD
F F T F                              $ PCHCDS NASTAM STOMAS
STOINV
F F F T                              $ FRWTFL FRWTGE FRWTGR
FRESUR
F T F F                              $ RENUMB STOGMT ROTGEO
ROTQUA
F F F F                              $ PRTCOE STRMAS SPHERE
ROTSYM
F F F F                              $ OCTMOD CAVFLU FRWTFV
INTCAV
F T                                  $ BOTREF MASREF
0 65808 0 6186                       $ NSTRC NSTRF NGEN NGENF
0 0 0                                $ NBRA NCYL NCAV
0.935E-4 59428.8                     $ RHO CEE
1. 1.                                $ CQ(1) CQ(2)
0. -1. 0. 0.                         $ DHALF CXHF CYHF CZHF
36. 0. 1. 0.                         $ DEPTH CXFS CYFS CZFS
14.7 386.4                           $ PATM GRAVAC
1                                    $ NSRADI
0. 0. 1 6186 1                       $ RAD1 RAD2 JBEG JEND JINC
0                                    $ NSORDR

AUGMAT DATA FOR FSP
strnam flunam geonam prenam          $ STRNAM FLUNAM GEONAM
PRENAM
F F F F                              $ FRWTGE FRWTST FRWTFL
LUMPFM
F F F T                              $ FLUSKY DAAFRM SYMCON
DOFTAB                                         -
```

```
F F F F                                     $ PRTGMT PRTTRN PRTSTF
PRTAUG
F F F F                                     $ MODTRN STRLCL INTWAT
CFADYN
11                                          $ NTYPDA
65808 197424 3 3                            $ NSTR NSFR NFRE NFTR1
1                                           $ NSETLC
0 1 6186 1                                  $ NDICOS JSTART JSTOP JINC


TIMINT DATA FOR FSP
prenam posnam                               $ PRENAM POSNAM
resnam                                      $ RESNAM WRTNAM
F T F F                                     $ REFSEC FLUMEM XXXXXX
XXXXXX
1                                           $ NTINT
0.0 0.00002                                 $ STRTIM DELTIM
T F F F                                     $ EXPWAV SPLINE VARLIN
PACKET
F T F F                                     $ HYPERB EXPLOS DOUBDC
VELINP
F F F F                                     $ BUBPUL SHKBUB XXXXXX
XXXXXX
1                                           $ NCHARG
0.                                          $ HYDPRE
0. -252.0 -336.0                            $ XC YC ZC
0. -108.0 -336.0                            $ SX SY SZ
201                                         $ JPHIST
1. 0.                                       $ PNORM DETIM
0.682E-5                                    $ DTHIST
1                                           $ CHGTYP
60. 12.0 24.0                               $ WEIGHT SLANT CHGDEP
99999 99999                                 $ NSAVER NRESET·
0 0 0 0                                      $ LOCBEG LOCRES LOCWRT
NSTART
F F F F                                     $ FORWRT STBDA2 ASCWRT
XXXXXX
0.0 -14.4 -108.0                            $ XV YV ZV
288. 0. 1. 0.                               $ DEPTH CXFS CYFS CZFS
14.7 386.4                                  $ PATM GRAVAC
F                                           $ DISPLA
```

LS-DYNA INPUT DECK:

```
*KEYWORD
*TITLE
HALF-MODEL OF FSP W/MAT 90 FLUID (ORIGINAL SIZE MODEL)
*CONTROL_TERMINATION
0.080,0,0,0,0
*CONTROL_TIMESTEP
0.00002,0.8,0,0,0,1,0
*CONTROL_OUTPUT
1,0,1,0,0,1,1
*CONTROL_PARALLEL
```

```
2,0,1
*DEFINE_CURVE
1
0,0.00002
0.080,0.00002
*DATABASE_HISTORY_NODE
225,728,1576,1615,2445,2471,1005,1609
1868,3815,6890,19819,22885
*DATABASE_NODOUT
0.00002
*DATABASE_BINARY_D3PLOT
0.0002
*DATABASE_BINARY_D3THDT
0.0002
*DATABASE_EXTENT_BINARY
0,0,3,1,1,1,1,1
0,0,0,0,0,0
*BOUNDARY_USA_SURFACE
2,1,0
*INITIAL_DETONATION
-1,0.0,-252.0,-336.0,0.0
6204.63,0.2891E-03,0.0,-108.0,-336.0,25072
$
$ NODES
$
*NODE
1,5.99997997,72.0000000,90.0000000,0,0
.
.
.
.
*PART
1
1,1,1,0,1
*SECTION_SHELL
1,2,1.0,3
1.000E+00,1.000E+00,1.000E+00,1.000E+00
*ELEMENT_SHELL_THICKNESS
1,1,1005,1121,1122,1111
1.000E+00,1.000E+00,1.000E+00,1.000E+00
.
.
.
.
*PART
2
2,2,2,0,2
*SECTION_SHELL
2,2,1.0,3
1.000E+00,1.000E+00,1.000E+00,1.000E+00
```

```
*ELEMENT_SHELL_THICKNESS
1161,2,1628,1630,1785,1783
1.000E+00,1.000E+00,1.000E+00,1.000E+00
 .
 .
 .
 .
*PART
3
3,3,3,0,3
*SECTION_SHELL
3,2,1.0,3
5.000E-01,5.000E-01,5.000E-01,5.000E-01
*ELEMENT_SHELL_THICKNESS
1465,3,1576,1712,1734,1580
5.000E-01,5.000E-01,5.000E-01,5.000E-01
 .
 .
 .
 .
*PART
4
4,4,4,0,4
*SECTION_SHELL
4,2,1.0,3
0.50,0.50,0.50,0.50
*ELEMENT_SHELL_THICKNESS
2169,4,2463,2466,2300,2460
5.000E-01,5.000E-01,5.000E-01,5.000E-01
 .
 .
 .
 .
*PART
90
90,90,90
*SECTION_SOLID
90,8
*ELEMENT_SOLID
1,90,310,316,204,305,3670,3671,3672,3673
 .
 .
 .
 .
$
$ MATERIAL CARDS
$
$ DEFINITION OF MATERIAL     1   PSHELL bottom_side
$
*MAT_ELASTIC
1,7.320E-04,3.000E+07,0.300
*HOURGLASS
1,5
$
$ DEFINITION OF MATERIAL     2   PSHELL dryside
```

```
$
*MAT_ELASTIC
2,7.320E-04,3.000E+07,0.300
*HOURGLASS
2,5
$
$ DEFINITION OF MATERIAL     3   PSHELL inner_bottom
$
*MAT_ELASTIC
3,8.200E-04,3.000E+07,0.300
*HOURGLASS
3,5
$
$ DEFINITION OF MATERIAL     4   PSEHLL stiffs
$
*MAT_ELASTIC
4,8.800E-04,3.000E+07,0.300
*HOURGLASS
4,5
$
$ DEFINITION OF MATERIAL     90   PSOLID water
$
*MAT_ACOUSTIC
90,9.35E-05,59428.8,0.5,1.0,14.7,386.4
0.0,36.0,-96.0,0.0,1.0,0.0
$
$ Face set daa_bdry
$
*SET_SEGMENT
2
6729,6730,6731,6732
.
.
.
.
$
$ RAYLEIGH DAMPING
$
*DAMPING_PART_STIFFNESS
1,0.5E-05
2,0.5E-05
3,0.5E-05
4,0.5E-05
*END
```

APPENDIX C. HELPFUL FEATURES IN MSC/PATRAN

MSC/PATRAN [Ref. 14] is a powerful finite element modeling and visualization tool. The program has many useful features to aid in visualizing and manipulating a finite element model. Different input and output formats are also supported, such as LS-DYNA keyword format. Basic familiarity with MSC/PATRAN is assumed. Important menu selections are featured in bold.

1. Creating **GROUPS** is useful for visualization of a complex mesh. The model can in effect be "sliced" into different sections for example and each put in a different group. The **CREATE** option is used to form a group. A group name must be entered. Elements to add to a group can then be selected with the mouse from the viewport. When selecting elements to add to a group, visible elements only can be selected by toggling the visible only button on the top left of the selection tool bar. This is only effective when using the hide view of the mesh (vice wireframe). The visible elements only selection feature is most useful when defining the wetted surface of a model. The **MODIFY** option provides for additions or removals from the target group. The target group can be changed with the **CHANGE TARGET** button. The **POST** option allows individual groups to be displayed in the current viewport. More than one group can be selected for display. The **shift** key must be held down to make multiple selections. This feature works also when selecting individual elements from the viewport. An individual element is selected, then, if additional elements are desired to be selected, they can be added to the list by holding down the shift key while highlighting them with the mouse.

2. A model can be moved in set increments using the **TRANSFORMATIONS** options found under the **VIEWING** menu. This option provides for rotation of the model about one of the three axes in a set fashion. The model can also be moved in set increments in any of the six main directions (x,y, and z). This provides for precise control over the model's positioning and aspect.

3. Multiple viewports can be created and posted using the **VIEWPORT** menu. The **CREATE** option allows the user to create and name a new viewport. Each created

viewport can be posted/unposted using the **POST** menu. The **MODIFY** menu provides for the current and default viewports to be changed. The current viewport is the "active" viewing window and it is where all actions performed will take effect. Groups can also be posted/unposted from this menu option. This effects the current viewport. The **TILE** option automatically places two displayed viewports side by side.

4. The **LIST** creation option under the **TOOLS** menu provides the means to find objects (elements, nodes, etc.) with a common **ATTRIBUTE** or **ASSOCIATION** with other objects (such as groups or certain elements). FEM or geometry can be chosen. Nodes or different element types can be specified for association or attribute selection. For example, an empty group can be created (the group name is entered in the group create dialog box and apply is depressed; no elements are selected from the viewport) and then a list can be created of all the elements with a common attribute, such as a particular material property or property set. The list of elements can then be added to the newly created group and subsequently displayed. The list can also be added to any existing groups. The list can be output to one of two sub-windows, **A** or **B**. The destination window is selected via the radial buttons at the bottom of the create list window. The list tool can be a very powerful asset.

5. The **DISPLAY** menu option provides a number of menu selections. The **PLOT/ERASE** option provides the means to "unclutter" the display viewport. Specific element types can be selected and then erased from the display. The erased elements are not deleted from the model; they are only removed from view. They can then be re-posted to the viewport by selecting the **PLOT ALL POSTED FEM OPTION**. All the objects in the viewport can also have their labeling toggled on and off via the appropriate menu selection. The object color can also be changed from the set default color. This is accomplished by simply clicking the small color patch next to the object name in the appropriate label selection menu. A small window of color choices will pop-up and a new color can be selected and applied the object.

6. The **FINITE ELEMENT** radial button has a number of useful mesh creation and diagnostic tools, one of which is the **VERIFY** option. By selecting **ELEMENTS** and **NORMALS,** element normal vectors can be displayed and even reversed if required. For the reverse option, a reference element must be designated. The **ELEMENTS/DUPLICATES** option allows any duplicate elements to be highlighted and deleted if the user desires. Either the higher or lower ID number element can be selected for deletion. **EQUIVALENCE** allows a tolerance to be set and any nodes falling within the tolerance will be merged and the database numbering reset. Nodes can be designated for exclusion from the equivalencing. The **RENUMBER** option allows nodes and/or elements to be renumber starting with a user specified number. The **SHOW** option displays the selected node's coordinates and ID number, and for elements the ID number, type, and property set is displayed. The selected nodes and elements are highlighted in the viewport if the ID number is input by hand rather than selected with the mouse.

7. Selecting the **LOADS/BCS** radial button allows creation of pressure load to define the wetted surface. When inputting the pressure set data, one has choices of top or bottom of the element (for two-dimensional elements). The correct choice is top, since this is the side with the normal vector pointing outward. For three-dimensional elements, such a fluid elements, the pressure load can be applied to free faces only (a button on the selection tool bar). This is useful for defining the outside surface of the fluid mesh for the DAA boundary. The visible only button should also be depressed when defining a wetted surface.

8. Results from a NASTRAN analysis can be input into PATRAN by selecting the **ANALYSIS** radial button, followed by choosing **READ OUTPUT2** under the action menu. The desired results file name can then be selected and read in by clicking the apply button.

9. The imported results can then be viewed using the **RESULTS** button. If the results are in a form that can be plotted in an xy-plot, then the results type should be changed from **BASIC** to **ADVANCED**. Under **RESULT CASE OPTIONS**, the desired results should be selected (highlighted), then the **GET RESULTS** bar

61

depressed. Under the **PLOT TYPE** menu, **XY-PLOT** can be selected. **PLOT TYPE OPTIONS** is used next to assign the global variable (usually time) and then the desired y-variable (such as displacement, velocity, and acceleration, depending on the results read in) can be selected to be plotted. The nodes whose response is desired can be input. Once the results curves are plotted, they can be further manipulated using the **XY** data radial button.

10. The **XY** data button has the normal menu selections, such as **CREATE, DELETE, MODIFY, POST**. These choices have options for both xy-windows and curves. Using create, new xy-windows can be generated and displayed with the post option. Curves cannot be generated here, they must be generated as in step 9 above. Curves can be deleted here and posted/unposted to/from different xy-windows.

11. ASCII files can be created from the generated curve data. Under the **xy** menu, **MODIFY/CURVE** should be selected. The desired curve is then selected (highlighted) from the middle window (which displays all of the curves currently created in the database file). The **DATA FROM KEYBOARD** option should be chosen and the **WRITE XY DATA TO FILE** button should be clicked on. Once apply is clicked, a filename can be input for the ASCII file and the destination directory selected. PATRAN does put a small text header in the file above the first xy-data pair. This header must be deleted prior to importing the file into UERD Tool.

12. The **PRINT** option can be found under the **FILE** menu. The user must be careful when printing to select what is to be printed. The top bar of the print menu can be toggled between either **CURRENT VIEWPORT** printing or **CURRENT XY-WINDOW** printing. **ALL VIEWPORTS** or **ALL XY-WINDOWS** can also be chosen. Color or black&white can be toggled under the print **OPTIONS** menu. Under options is where the print to file option is chosen and a filename is input. PATRAN can output postscript or encapsulated postscript files. The **PAGE SETUP** menu provides for selection of page orientation and size, as well as turning borders on and off. The output is not created until the apply button is clicked. It should also be noted that the output file name need not be changed for subsequent print views.

PATRAN automatically appends a sequentially numbered suffix to the postscript filename with each print output.

13. **NEUTRAL** files can be generated by selecting the **EXPORT** option under the **FILE** menu. Neutral files can be imported into PATRAN using the **IMPORT** option. PATRAN by default looks for a .out extension on neutral files.

APPENDIX D. FLUID MODELING USING TRUEGRID

This appendix covers the procedure for creating a fluid finite element mesh using TrueGrid's extrusion feature: the **BLUDE** command. The basics of using TrueGrid will not be covered here and some familiarity with the code is assumed. Additional information can be found in the TrueGrid user manual [Ref. 12].

Essentially the **BLUDE** feature pulls or "extrudes" the structural mesh through a "guide" mesh mated to the structural wetted surface in the form of a block part. The block part is actually attached to a surface definition created from a faceset of the wetted elements of the structural mesh. The resulting extruded mesh matches exactly to the structural mesh, a prerequisite for successful fluid modeling.

The extrusion procedure is as follows, with important commands and menu selections denoted in bold and all capital letters for emphasis:

1. A structural model must be created. TrueGrid can be used or the **READMESH** command can be used to input a mesh from another code format, such as LS-DYNA or NASTRAN. It is very important to remember though, that when TrueGrid reads in a finite element mesh from an outside code format, it renumbers ever element and grid point. Therefore, once the mesh is through being manipulated in TrueGrid, and it is written an output file, the grid point and element ID numbers will not match between the original and newly output model from TrueGrid (even if the original model was not modified in TrueGrid).

2. The elements of the structural model that will be in contact with the fluid, i.e. the wetted surface, must be grouped into **FACESETS**. This option can be accessed from the environment window under the **PICK** option by choosing the **SETS** button. The **FACES** button should be selected. Each "face" of the structural model should be put in a separate faceset, meaning each side, bottom, bow, and stern should be grouped individually. The reason for this will be clear once the procedure is understood and used. The **HIDE** drawing mode vice **WIREFRAME** should be used for the mesh to ensure that only the visible elements are picked. This will make faceset selection must easier, since it must be done by hand using the lasso tool guided by the mouse. The four-node selection option is the best to use when

choosing the faceset. This means that four nodes of an element must be within the selection lasso for the element to be added to the faceset. The selected elements will be highlight in white. If some elements are selected that are not desired in the particular set, they can be easily selected and removed; using the one node selection option is best for this operation. The **REMOVE** button should be pushed also. The set must be named and saved once selected.

3. The **SURFACE** menu **SD** (surface definition) option should be chosen next. A surface number must be input. The faceset option should be selected from the end of the surface options list and the name of the desired faceset should then be input. This step converts the named faceset into a surface definition. The new surface will be displayed in red in the physical window.

4. Next, the **PARTS** menu should be selected and the **BLUDE** option chosen. Using this option, the user creates a block part that will be attached to the above created surface. This block will serve as the "guide" for the extrusion of the structural mesh; therefore, the block's mesh must match the structural mesh or be of finer quality in order to get a quality extrusion; an exact match is not required however. This block part is created in the same way as a block using the **BLOCK** command. The blude command requires two additional inputs, however. First, the face of the block where the extrusion begins must be input. This is simply the face closest to the structure. Next, the name of the faceset to be extruded must input.

5. The block part created must now be attached to the surface created in step 3. It can be attached using any of TrueGrid's available options. The easiest being selection of the face to be attached and then selecting the surface and clicking the **PROJECT** button in the environment window. This will work for simple cases, but a complex surface may require use of other TrueGrid methods.

6. The interface of the extrusion mesh and the structural mesh should be carefully examined. Orthogonality of the fluid and structural mesh is a must (next to the wetted surface) and should be verified; TrueGrid's **DIAGNOSTICS** menu provides the necessary tools. The block mesh can be modified as needed using various TrueGrid tools to ensure a quality mesh is constructed for the extrusion; two

examples of useful tools are the mesh relaxation algorithms and use of a cubic spline to added curvature to the block mesh edges. Material properties can be assigned to the mesh also, just as with any other part in TrueGrid. In short, the extrusion mesh should be treated as any other part one would create in TrueGrid; all of the same options are available.

7. Once the user is satisfied with the extrusion mesh, the **MERGE** command should be used to end the **PARTS** phase and actually perform the extrusion. The result will be a fluid mesh, which matches exactly to the structural mesh. The mesh will consist of 8-noded solid elements. The **STP** option can be used also if required to ensure that the fluid mesh is merged with the structural mesh and there are no duplicate nodes. Additionally, prior to merging, the extrusion mesh can be replicated using the **LCT** and **LREP** commands. This will only be effective if the model is symmetric. Using these part replication features, the user only has to build one-half of the extrusion mesh.

8. Additional extrusions can be performed, including on any newly extruded mesh surfaces. This must usually be done to fully form a fluid mesh around the structural model.

9. Postscript images of the model and the mesh can be made using the **POSTSCRIPT** command. The command postscript is given at the command prompt with a the desired output filename. The **DRAW** button in the environment window should then be clicked to redraw the image. This creates the postscript file. Additional files will be generated as long as the command is active and the model is manipulated in any way so that it must be regenerated in the display window. The postscript command can be turned off by typing **POSTSCRIPT OFF**. One additional command that is quite useful in generating quality image files is the **RESO** command. The reso command is entered prior to the postscript command. The syntax is the command followed by a number that is the desired resolution. This is system limited. A resolution of 2300 has been used with success. The postscript files generated are black and white only, but they consist of vector data. This means the images generated are crisp and very accurate.

APPENDIX E. USEFUL FEATURES IN LS-TAURUS

TAURUS is an interactive post-processor and three-dimensional visualization tool for LS-DYNA [Ref. 16]. TAURUS has many useful features for viewing and manipulating model output responses obtained from LS-DYNA/USA simulations; a few of these features are detailed here. All TAURUS commands are fully documented in Appendix K of Reference 16. Basic familiarity with TAURUS is assumed.

1. A given state can be displayed in TAURUS by the following syntax: **s (state number) frin (fringe number)**. Note that the parentheses are not included (this syntax will be used to illustrate all commands); only the appropriate number is put in the command. In underwater shock simulations, pressure fringes are of concern; fringe 8 is pressure The fringe numbers for other variables are listed in a set of tables in Reference 16.

2. Animation can be easily set-up with the command: **r (starting state number) (final state number) (step) frin (appropriate fringe code)**. The animation can be set-up to run between any desired starting and ending state. The **gif** command allows a gif image to output of the currently displayed state in the visualization window. TAURUS names the file by default, pict#.gif (where the # is a consecutive integer starting at one for each gif image created during the current TAURUS session). The command **noborder** removes the border and text information from the visualization window. **Logo** toggles the drawing of the TAURUS logo. The command **cb** can be used to change the background color from the default black. After entering the command, the user must input the amount of red, green, and blue to be mixed for the desired background color. As an example, 0,0,0 is black, and 1,1,1 is white. Other colors can be made by experimentation. The command **cline** is used to change the mesh line color on the screen. The default is white. As with cb, the amount of red, green, and blue must be input.

3. A video tape of the resulting animation can be made by selecting the **video out** application from the SGI desktop list of media tools. Note that this feature must be installed and a VCR and TV must be hooked up to the SGI machine. The NPS SGI OCTANES have this option installed. The outline of a box will be visible on the

69

screen. This is the capture window outline for what is sent to the VCR/TV. The size of this window can be changed between two sizes: full screen and a somewhat less than full screen size. The size is changed by clicking on the video out gray box that appears on the screen. The flicker filter can also be toggled on and off in the same way, and the function can be turned off here too. The full screen size does not give the best output; it is better to use the smaller size for better quality on the TV end. The VCR can then be used to record the images transmitted from the computer.

4. Phase II of TAURUS is used to plot time histories of desired variables for elements and nodes. The procedure for making the plot is as followings (example is for element time history): first the command **elem (number of elements) (element numbers)** is used to designate the desired elements; next **gather** is used to read the element data into memory; once the gathering is complete the desired time history can be plotted with **etime (fringe number) (number of elements to plot) (element numbers to be plotted)**. The commands **aset (min) (max)** and **oset (min) (max)** can be used to set the x and y axes appropriately for the desired range. The **keep** command can be used to generate an ascii file with the plotted data in it. This command must be issued prior to the **etime** command and once entered the user is prompted to enter a filename for the output file. The ASCII file generated is in two column (x-y) format and contains the entire range of data for the element fringe requested (even if the data is only partially displayed in the plot window by use of the axis setting commands). It should be noted that this ascii file does contain some text header information above the data columns and the string "endplot" is placed at the end of the data.

LIST OF REFERENCES

1. Kelso, F.B. et. Al., "From the Sea, Preparing the Naval Service for the 21st Century", September 1992.

2. NAVSEA 0908-LP-000-3010A, *Shock Design Criteria for Surface Ships*, October 1994.

3. Military Specification, MIL-S-901D, Shock Tests, High Impact Shipboard Machinery, Equipment and Systems, Requirements for, March 1989.

4. OPNAV Instruction 9072.2, "Shock Hardening of Surface Ships", January 1987.

5. USS John Paul Jones (DDG-53) Shock Trial Final Report, AEGIS Program Manager (PMS-400), November 1994.

6. XYZ Scientific Applications, Inc., *TrueGrid®: A Quality Mesh in a Fraction of the Time*, Livermore, CA, 1997.

7. MacNeal-Schwendler Corporation, *MSC/PATRAN Installation and Operations Guide*, Version 7.0, Publication No. 903002, Los Angeles, CA, July 1997.

8. Cole, R.H., *Underwater Explosions*, pp. 3-13, Princeton University Press, 1948.

9. Shin, Y.S., "Naval Ship-Shock and Design Analysis", Course Notes for Underwater Shock Analysis, Naval Postgraduate School, Monterey, CA, 1996.

10. Geers, T.L., "Residual Potential and Approximate Methods for Three-Dimensional Fluid-Structure Interaction Problems", The Journal of the Acoustical Society of America, Vol. 49, pp. 1505-1510, 1971.

11. DeRuntz, J.A. Jr., "The Underwater Shock Analysis Code and Its Applications", Paper presented at the 60th Shock and Vibration Symposium, Vol. I, pp. 89-107, November 1989.

12. Hanselman, D. and Littlefield, B., *The Student Edition of MATLAB, Version 5 User's Guide*, Prentice Hall, 1997.

13. Livermore Software Technology Corporation, *LS-DYNA Keyword User's Manual*, Version 940, Livermore, CA, 1997.

14. Shin, Y.S., DeRuntz, J.A., "USA/LS-DYNA3D Software Training Course", Vol. V, July 1996.

15. DeRuntz, J.A. Jr. and Rankin, C.C., "Applications of the USA-STAGS-CFA Code to Nonlinear Fluid-Structure Interaction Problems in Underwater Shock of Submerged Structures", 60th Shock and Vibration Symposium Proceedings, Vol. I, November 1989.

16. ViewTech ASA, *Glview Users Guide, UNIX, Version 5*, Norway, 1998.

17. Wood, S.L., "Cavitation Effects on a Ship-Like Box Structure Subjected to an Underwater Explosion", Master's Thesis, Naval Postgraduate School, Monterey, CA, September 1998.

18. Arons, A.B., et al, "Long Range Shock Propagation in Underwater Explosion Phenomena II," Underwater Explosion Compendium, Vol. 1, October 1949.

19. Costanzo, F.A. and Gordon, J.D., "An Analysis of Bulk Cavitation in Deep Water," DTNSRDC, UERD Report, May 1980.

20. Stow, B.M. and Gordon, J.D., "Bulk Cavitation Caused by a Plane Shock Wave," DTNSRDC Report 84/047, October 1984.

INITIAL DISTRIBUTION LIST

<div align="right">No. Copies</div>

1. Defense Technical Information Center...2
   8725 John J. Kingman Rd., Ste 0944
   Ft. Belvoir, VA 22060-6218

2. Dudley Knox Library...2
   Naval Postgraduate School
   411 Dyer Rd.
   Monterey, CA 93943-5101

3. Professor Young S. Shin, Code ME/Sg 2
   Department of Mechanical Engineering
   Naval Postgraduate School
   Monterey, CA 93943

4. Naval/Mechanical Engineering Curricular Office (Code 34)..............................1
   Department of Mechanical Engineering
   Naval Postgraduate School
   Monterey, CA 93943

5. LT James R. Smith...2
   256 Tunisia Road
   Seaside, CA 93955

6. Michael C. Winnette 1
   Carderock Division
   Naval Surface Warfare Center
   9500 MacArthur Blvd.
   West Bethesda, MD 20817-5700

7. Gust Constant...1
   PMS400D5
   Naval Sea Systems Command
   2531 Jefferson Davis Highway
   Arlington, VA 22242-5165